Transient Theory of Pumping Induced Depletion and Drawdown of a Stream with Finite Channel Storage

Bwalya Malama[1], Ying-Fan Lin[2], Hwa-Lung Yu[2], Hua-Ting Tseng[2], and Sam Greene[1]

[1]Natural Resources Management and Environmental Sciences, California Polytechnic State University, San Luis Obispo, State of California, USA

[2]Department of Bioenvironmental Systems Engineering, National Taiwan University, Taipei City, Taiwan

Correspondence: Bwalya Malama (bmalama@calpoly.edu)

Abstract. Mathematical models for groundwater pumping induced stream depletion with concomitant transient stream stage decline or drawdown are developed in this work to address a deficiency in existing models, namely, the use of a fixed-stage boundary condition or source term at the stream-aquifer interface. Existing approaches in the hydrogeology literature enforce a fixed stream stage condition during pumping by prescribing a constant-head or a general boundary condition or source term, both of which imply that the stream is an infinite water source and can replenish the aquifer indefinitely during groundwater pumping. It is a major limitation of the model, as it ignores the most observable adverse effect of long-term groundwater abstraction through well in close proximity to streams, namely stage declines that can eventually lead to dry streambeds. **Field data are presented to demonstrate that stream stage decline does indeed occur in response to groundwater pumping pumping near hydraulically connected streams, motivating the development of an alternative theory that predicts stream depletion with transient stream drawdown. The theory is based on the concepts of finite stream storage and the mass continuity principle at the stream-aquifer interface, and is used to develop models for cases of a non- and a fully-penetrating stream. The proposed models are shown to reduce to existing fixed-stage models in the limit as stream storage becomes infinitely large, and to the confined aquifer flow with a no-flow boundary at the streambed when the stream storage vanishes. The models are then applied to field observations of both aquifer and stream drawdown, yielding estimates of aquifer hydraulic parameters as well as streambed conductance and a finite stream storage coefficient. The observed and model-predicted transient drawdown behavior indicate that existing fixed-stage models (a) underestimate late-time aquifer drawdown and (b) overestimate the available recharge from streams to pumping wells, which has significant implications for the sustainable management of groundwater resources.**

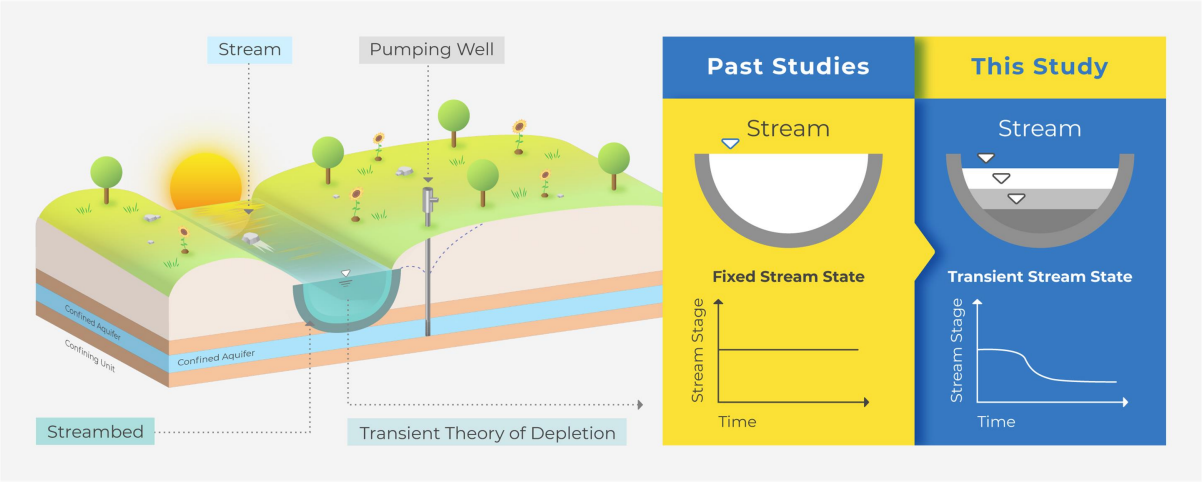

. Graphical Abstract. Schematic illustrating the proposed theory of stream stage that shows transient response to pumping.

1 Introduction

Groundwater pumping in basins with or bounded by streams can lead to reduced stream flows, with undesirable impacts on both human use and ecosystem function (Winter et al., 1998; Bowen et al., 2007; Yu and Chu, 2010; Foglia et al., 2013; Zipper et al., 2018; Tolley et al., 2019; Kwon et al., 2020) due to drying up of streambeds and disconnected stream-groundwater systems. Theis (1941) was among the first to develop a model for stream depletion resulting from groundwater pumping from a confined aquifer, with depletion defined as the decrease in stream discharge. Theis (1941) used the earlier model of Theis (1935), developed for a laterally infinite aquifer, together with the principle of linear superposition, to simulate a constant-head (Dirichlet) boundary condition at the stream-aquifer interface and develop a model for stream depletion. Glover and Balmer (1954) extended upon this work with a closed-form function of the model, later tabulated by Jenkins (1968). Hantush (1965) made the next notable advancement by introducing a semi-pervious streambed with a general (Robin) boundary condition at the stream-aquifer interface, where the flux across the streambed was treated as being proportional to the differential head across the streambed thickness, with stream stage held constant. Intaraprasong and Zhan (2009) expanded upon this work, solving the full groundwater flow equation throughout the streambed with stream stage prescribed as a time-dependent function. Chan (1976) and Asadi-Aghbolaghi and Seyyedian (2010) generalized application of the superposition principle to confined aquifer flow domains bounded laterally by intersecting streams. Other workers have extended these analytical stream depletion models to cases of partially penetrating streams (Grigoryev, 1957; Bochever, 1966; Zlotnik et al., 1999; Hunt, 1999; Butler Jr et al., 2001; Fox et al., 2002; Butler Jr et al., 2007; Zlotnik and Tartakovsky, 2008). Stream depletion models for cases where the aquifer is unconfined have been developed by Hunt (2003, 2009), who also uses a fixed-stage condition with a Robin-type boundary condition or source function.

Numerical models, such as MODFLOW (Harbaugh, 2005) and MIKE SHE (Refsgaard et al., 2010), through their respective stream packages, treat stream boundary conditions and source/drainage terms in a manner similar to the analytical models

discussed above. They also allow one to specify the spatially variable stream stage using empirical hydrographs (Harbaugh, 2005) or formulas such as the Manning equation (Prudic et al., 2004) to allow for effect of stream flow. The approach is highly nonlinear, requiring iterative methods at every time step, which can be computationally taxing. A comprehensive review of the literature on different configurations of pumping-induced stream depletion problems has been provided by Huang et al. (2018), where the Dirichlet and Robin boundary conditions are identified as the only ones used for such problems. To reiterate, where source terms are introduced in partially-penetrating stream scenarios, they are treated as linear functions of the differential head across the streambed, with fixed stage.

As mentioned already, the models discussed above use either a constant-head or Robin boundary condition (or source term) at the stream-aquifer interface, both of which require fixed (or more generally, prescribed) stream stage with the stream acting as an infinite source of storage that can supply recharge indefinitely during periods of groundwater pumping. However, it is intuitively clear that streams can only provide a limited amount of recharge and for only a limited period of time to pumping wells. This has been recognized by others, including Zlotnik (2004), who subsequently introduced the concept of maximum stream depletion rate (SDR). As a consequence of their limited capacity to provide recharge during groundwater pumping, streams can undergo transient stream stage decline or drawdown in addition to depletion. According to Kollet and Zlotnik (2003), stream stage decline due to aquifer pumping can only be ignored in cases where the stream flow rate is two orders of magnitude or more higher than the pumping rate. This suggests that new models that consider finite stream storage and the associated transient stage drawdown response to pumping are required when the stream flow rate is small or comparable to the pumping rate.

Given the limitations of the stream depletion models reviewed above, an alternative theory is proposed here where a new boundary condition is imposed at the stream-aquifer interface by invoking the mass-balance principle and introducing the concept of finite stream channel storage. Hence, in this study, two semi-analytical models are developed for the cases of non- or minimally-penetrating streams (NPS) and fully-penetrating streams (FPS) in a confined aquifer, taking into account the effect of finite stream channel storage and the resulting drawdown of the stream. It is reiterated again here that stream drawdown is distinguished from stream depletion because it defines a decline stream stage whereas the latter only refers to a decrease in stream discharge rate. The model developed herein are the first semi-analytical models in the hydrogeology literature to accomplish this, overcoming the limitation of existing analytical models that assume streams to have fixed-stage. The solutions are validated by comparing them with a numerical model based on the finite-element method (FEM) and with field observations of aquifer and stream drawdown. Finally, the newly developed models are applied to field observations of stream and aquifer drawdown in a parameter estimation exercise by fitting the models to both aquifer and stream drawdown data, which demonstrates their practical application.

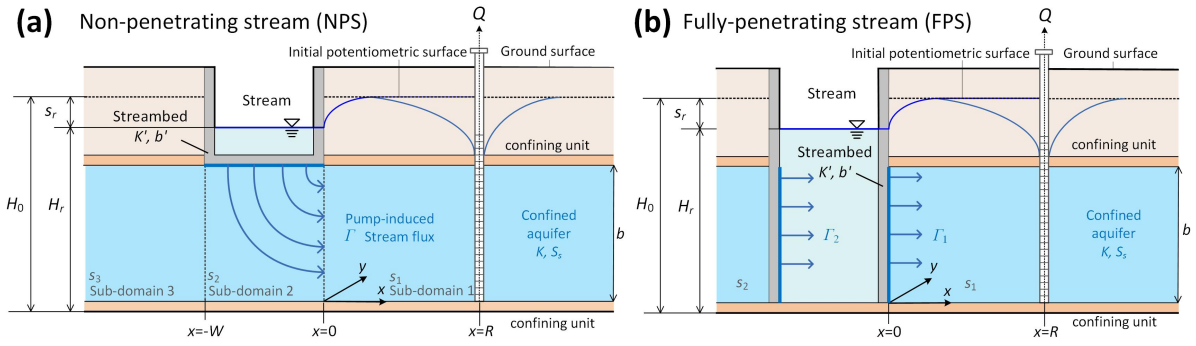

Figure 1. The schematic diagram of the conceptual model of the stream-aquifer system used for the (a) non-penetrating stream (NPS) and (b) fully-penetrating stream (FPS) models derived herein.

2 Methods

In the following, we describe the mathematical formulation and the proposed new boundary condition, develop semi-analytical solutions for the two cases already mentioned above, and apply the model to field observations of stream and aquifer drawdown.

2.1 Governing Equations of Flow

We consider a stream with finite storage and derive two solutions that allow the stream stage to respond to pumping. To do this, we consider flow to a fully-penetrating well in a confined aquifer in the neighborhood of a non-penetrating stream (NPS) and a fully-penetrating stream (FPS). For the FPS, we consider two cases: one in which flow in the aquifer on both sides of the stream is considered, and one in which only flow in the aquifer on the side of the pumping well is considered. We assume that groundwater is pumped at a constant rate, Q [$\mathrm{L^3T^{-1}}$], from a line-sink located at a distance of R [L] from the stream bank. The aquifer has infinite lateral extent away from the stream, with a uniform thickness b [L] and anisotropic horizontal hydraulic conductivities K_x and K_y [$\mathrm{LT^{-1}}$] in the x- and y-directions, respectively. The aquifer interacts with the stream across a streambed with hydraulic conductivity K' [$\mathrm{LT^{-1}}$] and thickness b' [L] (conductance $\beta = K'/b'$) as in Hantush (1965). The effects of streambed storage are neglected, and the focus is only on the effects of stream channel storage. Stream stage, $H_r(y,t)$ [L], is relative to the bottom of the aquifer. Stream drawdown is defined as $\mathbf{s_r}(\mathbf{y},\mathbf{t}) = \mathbf{H_0} - \mathbf{H_r}(\mathbf{y},\mathbf{t})$, where H_0 [L] is the initial stream stage, which is set equal to the initial aquifer hydraulic head. It should be noted here that aquifer head and stream stage are assumed to be measured relative to the same datum (base of aquifer in this work) and the stream-aquifer system is initially at equilibrium. The conceptual models of the problem described here are shown schematically in Figure 1.

The governing equation of confined flow problem considered in this work is (Fox et al., 2002)

$$S_s \frac{\partial s}{\partial t} = \mathbf{K}\nabla^2 s + f_s(x,y,t), \tag{1}$$

where $s = H_0 - h(x,y,t)$ is aquifer drawdown, (x,y) are spatial coordinates in the horizontal plane, t is the elapsed time from the onset of pumping, $\mathbf{K}$ is the diagonal aquifer hydraulic conductivity tensor with principal values K_x and K_y, S_s is aquifer

specific storage, and $f_s(x,y,t)$ is a sink/source function. The x coordinate axis is perpendicular to the stream bank with the origin on the stream bank closest to the pumping well. The y-axis is parallel to the stream channel axis and extends from $y=-\infty$ to $y=\infty$.

The aquifer flow problem is solved subject to the initial condition

$$s|_{t=0} = 0, \tag{2}$$

and the far-field boundary conditions

$$\lim_{\substack{x\to\pm\infty \\ y\to\pm\infty}} s = 0. \tag{3}$$

For simplicity, the stream-aquifer flow system is assumed to be initially at equilibrium. For cases where a background uniform flow field exists, the principle of superposition may be invoked to apply the solution developed herein.

2.1.1 Non-penetrating Stream

We first consider the case of a non-penetrating stream (NPS) that flows atop an aquifer to simulate the case where the stream has incised through the upper confining unit and only minimally penetrates the aquifer. The schematic of the conceptual model of this case in shown in Figure 1(a). To solve the flow problem, aquifer drawdown is defined in a piecewise manner as

$$s(x,y,t) = \begin{cases} s_1(x,y,t) & x > 0 \\ s_2(x,y,t) & x \in [-W,0] \\ s_3(x,y,t) & x < -W \end{cases} \tag{4}$$

where W is the width of the stream. Also, the sink/source function, $f_s(x,y,t)$, is defined as

$$f_s(x,y,t) = \frac{1}{b}\begin{cases} -Q\delta(x-R)\delta(y)/\pi & x > 0 \\ \Gamma & x \in [-W,0] \\ 0 & x < -W, \end{cases} \tag{5}$$

where Q is the pumping rate from a well located a distance R, from the stream bank along the x-axis, $\delta(\cdot)$ is the Dirac delta function, and Γ [LT^{-1}] is the mass-transfer function across the stream-aquifer interface through the base of the stream. The term $Q\delta(x-R)\delta(y)/\pi$ represents the well as a continuous line sink with its center located at $(R,0)$.

The mass-transfer function, Γ, across the streambed is expressed here as

$$\Gamma = \beta\left[s(x,y,t) - \mathbf{s_r}(\mathbf{y},\mathbf{t})\right], \;\; x \in [-W,0] \tag{6}$$

where β is the streambed conductance, defined as $\beta = K'/b'$, where K' is streambed hydraulic conductivity and b' is its thickness. **Note again the time dependence of stream drawdown, $\mathbf{s_r}(\mathbf{y},\mathbf{t})$, an unknown system state variable, to be solved for along with aquifer drawdown.**

Additionally, continuity conditions for drawdown

$$s_1|_{x=0} = s_2|_{x=0} \tag{7}$$

$$s_2|_{x=-W} = s_3|_{x=-W}\,, \tag{8}$$

and flux

$$\left.\frac{\partial s_1}{\partial x}\right|_{x=0} = \left.\frac{\partial s_2}{\partial x}\right|_{x=0} \tag{9}$$

$$\left.\frac{\partial s_3}{\partial x}\right|_{x=-W} = \left.\frac{\partial s_2}{\partial x}\right|_{x=-W}, \tag{10}$$

are enforced at $x = 0$ and $x = -W$.

It should be noted that for the NPS case vertical flow across the streambed is treated as a sink/source term in equation (5) defined by the mass-transfer function in equation (6), where stream stage and the associated drawdown are functions of both y and time t. This dependence on time is what distinguishes the present work from fixed stage models where stage is set as $h_r = H_0 =$ const. and stream drawdown vanishes identically ($s_r \equiv 0$). To allow for such a temporally variable stream stage and drawdown, an additional condition is required in the stream as discussed subsequently.

2.1.2 Fully-penetrating Stream

The second case considered is one where the stream has fully incised through both the thicknesses of the upper confining unit and the aquifer, a case commonly referred to in the hydrogeology literature as that of a fully-penetrating stream (FPS). A schematic of the conceptual model for this case is shown in Figure 1(b). Aquifer drawdown for this case is defined in a piecewise manner as

$$s(x,y,t) = \begin{cases} s_1(x,y,t) & x > 0 \\ s_2(x,y,t) & x < -W \end{cases} \tag{11}$$

when flow on the far-side half-space of the aquifer is accounted for. Here, $s_1(x,y,t)$ is the drawdown of the aquifer in the half-space with the pumping well, and $s_2(x,y,t)$ is the drawdown in the far side half space. For the case where the flow on the far-side $(x < -W)$ half-space is neglected, only the drawdown on the pumped half-space is considered. Such a case is realizable when the stream flows along a fault line where the far-side bank comprises an impermeable formation.

The boundary condition imposed at the stream-aquifer interface is specified as

$$-K_x \left.\frac{\partial s_1}{\partial x}\right|_{x=0} = \Gamma_1, \tag{12}$$

for the pumped half-space, and

$$-K_x \left.\frac{\partial s_2}{\partial x}\right|_{x=-W} = \Gamma_2 \tag{13}$$

on the far side, where the mass-transfer functions Γ_1 and Γ_2 are defined as

$$\Gamma_1 = -\beta\left[s_r(y,t) - s_1(x,y,t)\right],\ x = 0 \tag{14}$$

$$\Gamma_2 = \beta\left[s_r(y,t) - s_2(x,y,t)\right],\ x = -W \tag{15}$$

for the pumped-side and far-side stream-aquifer interfaces. Here, we assume that the two interfaces have the same conductance, β. For the case where flow in the far-side half-space is neglected, $\Gamma_2 \equiv 0$. Note that for this case, a boundary condition is imposed at the stream-aquifer interface. **Stream drawdown is again treated as a time dependent function, which necessitates an additional condition discussed in the following section.**

2.1.3 Accounting for Stream Drawdown and Channel Storage

As discussed above, the models of Hantush and Jacob (1955) and Fox et al. (2002) assume that the stream stage is fixed; the stream does not experience drawdown in response to groundwater pumping. Here, we develop a model that accounts for stream drawdown. It should be noted that the flow problem defined above is ill-posed for both the NPS and FPS cases because stream drawdown, $s_r(y,t)$, is left unspecified in both equations (6) and (14). If the stream is assumed to have fixed stage, as is the case in Hantush and Jacob (1955) and Fox et al. (2002), $s_r \equiv 0$. From the resulting Robin BC, one can recover both the no-flow and Dirichlet BCs at the stream-aquifer interface by setting $\beta = 0$ and $\beta \to \infty$, respectively.

In this work, we are concerned with the case where the stream stage does not remain fixed but is allowed to respond to pumping (see Figure 1a); the stream is allowed to undergo drawdown in response to aquifer pumping, in which case $s_r \neq 0$. We achieve this by specifying an additional condition at the stream aquifer interface, namely a mass-balance condition applied to the stream channel, which simply states that the rate of change of mass within the stream equals the rate of mass transfer across the streambed induced by pumping. In the following development of the theory, stream flow velocity is neglected for simplicity.

For the NPS model, this condition can be mathematically stated by the relation

$$C_r \frac{\partial s_r}{\partial t} = \Gamma, \tag{16}$$

whereas for the FPS model

$$C_r \frac{\partial s_r}{\partial t} = \Gamma_1 + \Gamma_2, \tag{17}$$

where $C_r \in [0,\infty)$ is a stream channel storage coefficient, defined as a dimensionless measure of the volume of water, δV_w, which flows through a unit area of the streambed, δA_r, per unit change in stream stage, δh_r (i.e., $C_r = \delta V_w/(\delta A_r \delta H_r)$). It is a measure of the volume contribution of water stored in the stream channel to aquifer flow, and is distinguished here from streambed elastic storage.

For a stream channel with an idealized uniform geometric cross-sectional structure, it is possible to provide simple expressions for this parameter. For example, in the FPS case, the stream channel has a rectangular cross section, with stream width

Table 1. Nomenclature.

Parameters/Variables	Definitions	Parameters/Variables	Definitions
A	$1.73\sqrt{\alpha}$ [$\mathrm{LT}^{-1/2}$]	s	Aquifer drawdown [L]
b	Thickness of a confined aquifer [L]	s_{obs}	Temporal drawdown observation [L]
b'	Thickness of a streambed [L]	s_r	Stream drawdown [L] defined as $H_0 - H_r$
C_r	Stream channel storage coefficient [-] and $C_r \in [0, \infty)$	t	Elapsed time [T] from the beginning of pumping
f_s	Sink/source function	t_n	Time [T] at n-th observation
F	Objective function	W	Width of the stream [L]
H_0	Initial stream stage [L] equal to the initial aquifer hydraulic head	(x, y)	Spatial coordinates [L] in the horizontal plane
H_r	Stream stage [L] relative to the aquifer bottom	Y	Set of parameter $\{K_x, S_s, \kappa, \beta, C_r\}$
K_x	Hydraulic conductivity [LT^{-1}] in x-direction	Y_{opt}	Set of parameters that minimizes the objective function
K_y	Hydraulic conductivity [LT^{-1}] in y-direction	α	Hydraulic diffusivity [$\mathrm{L}^2\mathrm{T}^{-1}$]
K'	Hydraulic conductivity [LT^{-1}] of streambed	β	Conductance [T^{-1}] defined as K'/b'
$\mathbf{K}$	Diagonal aquifer hydraulic conductivity tensor	γ	Euler's constant $\simeq 0.577216$
N	Total number of temporal drawdown observations	Γ	Mass-transfer function [LT^{-1}] across the stream-aquifer interface
q_r	Point-wise depletion flux [LT^{-1}]	δA_r	Unit area [L^2] of streambed defined as $2b\delta y$
Q	Pumping rate [$\mathrm{L}^3\mathrm{T}^{-1}$] in the pumping well	δH_r	Unit change [L] in drawdown
Q_r	Stream depletion rate [$\mathrm{L}^3\mathrm{T}^{-1}$]	δV_w	Unit volume of stream water [L^3] defined as $W\delta y\delta H_r$
R	Distance of pumping well [L] from the stream bank along the x-axis	δy	Unit distance [L] in y-direction
κ	Anisotropy ratio [-] in the horizontal plane defined as K_y/K_x		

W and aquifer thickness b, $\delta V_w = W\delta y\delta H_r$, $\delta A_r = 2b\delta y$, leading to $C_r = W/b$ if the mass exchange is limited to the stream bank. For the NPS case, where a similar simple geometric profile may be adopted for the cross section of the stream channel, it can be shown that C_r is of the order of unity. For more complex cross-sectional geometries of channels that vary spatially with y, the parameter C_r can be empirically estimated by inversion of the stream and aquifer drawdown data. It is also possible, in principle, to develop empirical functions relating C_r to the dimensionless ratio $\langle W \rangle / H_r$ of the form $C_r = f(\langle W \rangle / b)$, where $\langle W \rangle$ is some well-defined spatial (in y) average of stream width. Additional research outside the scope of the present work would be needed to develop such empirical relations. It is also easy to imagine the parameter C_r as a (non-linear) function of the stream stage. For our purposes here, adopting the principle of parsimony for mathematical tractability, we restrict the development of a solution to the case where C_r is a constant for the duration of a pumping test.

2.2 Analytical Solutions of the Flow Problem

To solve the flow problem described above, the governing equation is first transformed into a dimensionless form. Details of the nondimensionalization of the governing equations and their solutions may be found in the Appendix. The dimensionless variables and parameters that appear in the solution are defined in Table 2. Laplace and Fourier-cosine transforms are applied to the dimensionless governing equations, which are then solved by standard methods for ordinary differential equations. The respective inversion formulae of the transforms are finally used to numerically obtain the applicable flow solutions in space-time. The transform and inversion formulae can be found in standard textbooks of Engineering Mathematics, and interested readers may refer to the reference text of Haberman (2012). Similar solution approaches have been used in the hydrogeology literature by Butler Jr et al. (2001) and others.

2.2.1 Non-Penetrating Stream

The exact solution for aquifer drawdown, in transform space, for the NPS case can be shown (see Appendix for details) to be

$$\tilde{\tilde{s}}_D = \frac{2e^{-\eta}}{p\Delta_1}\begin{cases} e^{\eta(1-x_D)}\tilde{\tilde{g}}_1(p,\xi,1.0) & \forall x_D > 1 \\ \tilde{\tilde{g}}_1(p,\xi,x_D) & \forall x_D \in [0,1] \\ \hat{\eta}\cosh[\hat{\eta}(x_D+W_D)] + \eta\sinh[\hat{\eta}(x_D+W_D)] & x_D \in (-W_D,0) \\ \hat{\eta}e^{\eta(W_D+x_D)} & x_D \le -W_D, \end{cases} \tag{18}$$

where $\tilde{\tilde{s}}_D$ is the Laplace and Fourier cosine transform of s_D, p is the Laplace transform variable, ξ is the Fourier cosine transform variable, and with

$$\eta = \sqrt{p+\kappa\xi^2} \tag{19a}$$

$$\hat{\eta} = \sqrt{\eta^2+\zeta} \tag{19b}$$

$$\zeta = \frac{p\beta_D}{p+\beta_D^*} \tag{19c}$$

$$\beta_D^* = \frac{\beta_D}{C_{D,r}} \tag{19d}$$

$$\Delta_1 = 2\hat{\eta}\eta\cosh(\hat{\eta}W_D) + \left(\eta^2+\hat{\eta}^2\right)\sinh(\hat{\eta}W_D), \tag{19e}$$

$$\tilde{\tilde{g}}_1(p,\xi,x_D) = \hat{\eta}e^{\eta x_D}\cosh(\hat{\eta}W_D) + \tilde{\tilde{g}}_2(p,\xi,x_D)\sinh(\hat{\eta}W_D), \text{ and} \tag{19f}$$

$$\tilde{\tilde{g}}_2(p,\xi,x_D) = \eta\cosh(\eta x_D) + (\hat{\eta}^2/\eta)\sinh(\eta x_D). \tag{19g}$$

Here, $\beta_D = \beta/(K_x/R) = (K'/K_x)/b'_D$ is the dimensionless stream conductance, $W_D = W/R$ is the dimensionless stream channel width, and $C_{D,r} = b_D(C_r/S)$ is the dimensionless ratio of the stream channel storage coefficient to aquifer storativity scaled by the normalized aquifer thickness.

The corresponding solution for stream drawdown is given by

$$\tilde{\tilde{s}}_{D,r} = \frac{\tilde{\tilde{s}}_D(p,\xi,x_D)}{1+p/\beta_D^*}, \quad x_D \in (-W_D,0), \tag{20}$$

where $\tilde{\tilde{s}}_{D,r}$ is the Laplace and Fourier cosine transform of dimensionless stream drawdown $s_{D,r}$. Upon inversion from transform space, Equation (20) may be used to compute stream drawdown induced by pumping from a well completed in a confined aquifer. Space-time stream and aquifer drawdown are obtained by numerical inversion of the Fourier cosine and Laplace transforms using numerical quadrature and the Stehfest (1970) algorithm as implemented within the Wolfram Mathematica environment. The algorithms of numerical integral and Stehfest (1970) inversion written in the Mathematica script can be found in the hyperlink provided in acknowledgements.

Table 2. Definitions of dimensionless variables and parameters based on system characteristic length $L_c = R$, time $T_c = R^2/\alpha_x$ with $\alpha_x = K_x/S_s$, head $H_c = Q/(2\pi bK_x)$, and flux $q_c = K_x(H_c/R)$.

Symbols	Definitions	Symbols	Definitions
$s_{D,i}$	s_i/H_c	κ'	K'/K_x
$s_{D,r}$	s_r/H_c	β_D	$\beta R/K_x = \kappa'/b'_D$
x_D	x/R	β^*_D	$\beta_D/C_{D,r}$
y_D	y/R	$C_{D,r}$	$b_D C_r/S$
t_D	t/T_c	W_D	W/R
b_D	b/R	q_D	$2\pi bRq/Q = q/q_c$
b'_D	b'/R	$Q_{D,r}$	Q_r/Q
κ	K_y/K_x		

2.2.2 Fully-Penetrating Stream

As detailed in Appendix D, the exact aquifer drawdown solution for the FPS model, allowing for flow on both sides of the stream, is given by

$$\tilde{\tilde{s}}_D = \frac{2e^{-\eta}}{p\Delta_2}\begin{cases} e^{-\eta(x_D-1)}\tilde{\tilde{g}}_3(p,\xi,1.0) & \forall x_D > 1 \\ \tilde{\tilde{g}}_3(p,\xi,x_D) & \forall x_D \in [0,1] \\ p\beta_D\beta^*_D e^{\eta(W_D+x_D)} & x_D \le -W_D, \end{cases} \tag{21}$$

where $\tilde{\tilde{s}}_D$ is the Laplace and Fourier cosine transform of aquifer drawdown, s_D,

$$\tilde{\tilde{g}}_3(p,\xi,x_D) = \chi_1\cosh(\eta x_D) + \chi_2\sinh(\eta x_D), \tag{22}$$

$$\chi_1 = \frac{\Delta_2}{\beta_D+\eta} + p\beta^*_D\beta_D, \tag{23}$$

$$\chi_2 = \frac{\beta_D\Delta_2}{\eta(\beta_D+\eta)} - p\beta^*_D\beta_D, \text{ and} \tag{24}$$

$$\Delta_2 = p(\beta_D+\eta)\left[2\beta^*_D\eta + p(\beta_D+\eta)\right]. \tag{25}$$

The corresponding stream drawdown solution in transform space is

$$\tilde{\tilde{s}}_{D,r}(p,\xi) = \frac{2e^{-\eta}}{p\Delta_2}\frac{\beta^*_D\left(\chi_1 + p\beta_D\beta^*_D\right)}{p+2\beta^*_D}, \tag{26}$$

in transform space. The space-time solution, a function of t_D and y, is obtained numerically as stated previously.

When there is no flow across the far-side stream-aquifer interface, with $\Gamma_2 \equiv 0$, the solution reduces to

$$\tilde{\tilde{s}}_D = \frac{2e^{-\eta}}{p\Delta^*_3}\begin{cases} \tilde{\tilde{g}}_5(p,\xi,x_D) & \forall x_D \le 1 \\ e^{-\eta x_D}\tilde{\tilde{g}}_5(p,\xi,1.0) & \forall x_D > 1 \end{cases} \tag{27}$$

where $\tilde{\bar{s}}_D$ is the Laplace and Fourier cosine transform of s_D, $\Delta_3^* = \eta + \zeta$, $\tilde{\bar{g}}_5(p,\xi,x_D) = \cosh(\eta x_D) + (\zeta/\eta)\sinh(\eta x_D)$, and ζ is as defined previously. The corresponding solution for dimensionless stream drawdown is

$$\tilde{\bar{s}}_{D,r}(p,\xi) = \left[1 - \chi\left(1 - \frac{1}{\eta p \beta_D}\right)\right]\frac{e^{-\eta}}{p\Delta_3^*}, \tag{28}$$

which upon inversion gives dimensionless stream drawdown, $s_{D,r}(y_D,t_D)$ as a function of time, t_D, and position along the stream channel, y_D. As mentioned previously, the inversion from transform space is performed numerically in the Wolfram Mathematica as well as using MATLAB functionality and scripts.

2.2.3 Stream Depletion Solution

Stream depletion, Q_r [$\mathrm{L^3T^{-1}}$], defined as the volume rate of flow captured from the stream by a pumping well, is obtained simply by integrating the point-wise streambed flux along the length of the stream. The point-wise depletion flux, q_r, in dimensionless form, is

$$q_{D,r} = C_{D,r}\frac{\partial s_{D,r}}{\partial t_D} \tag{29}$$

where $q_{D,r} = q_r/(2\pi bR/Q)$. In the Laplace- and Fourier-cosine transform domain, equation (29) becomes $\tilde{\bar{q}}_{D,r} = pC_{D,r}\tilde{\bar{s}}_{D,r}$. Inverting the Fourier cosine inverse transform yields (Povstenko, 2015)

$$\bar{q}_{D,r} = pC_{D,r}\int_0^\infty \tilde{\bar{s}}_{D,r}\cos\xi x_D \, d\xi. \tag{30}$$

Therefore,

$$\bar{Q}_{D,r} = \frac{C_{D,r}}{\pi}\begin{cases} \displaystyle\int_0^\infty p\bar{s}_{D,r}\mathrm{d}y_D & \text{for FPS and} \\ \displaystyle\frac{1}{b_D}\int_0^\infty\int_{-W_D}^0 p\bar{s}_{D,r}\mathrm{d}x_D\mathrm{d}y_D & \text{for NPS,} \end{cases} \tag{31}$$

where $Q_{D,r} = Q_r/Q$. Equation (31) includes improper integrals, which can be time consuming to evaluate numerically. Additionally, there may be a practical limit on the stream reach that contributes appreciable amounts of water to the well over the pumping period. Hence, a definite integral over the interval $y_D \in [0, L_D]$, may be more practical. Using the late-time drawdown approximation of Cooper Jr and Jacob (1946), namely,

$$s_D = -\gamma/2 - \ln(u) \tag{32a}$$

$$u = \frac{r_D^2}{4\alpha t_D} \tag{32b}$$

$$r_D^2 = (x_D - 1)^2 + y_D^2. \tag{32c}$$

where s_D is dimensionless drawdown, α is the hydraulic diffusivity K/S_s, and $\gamma \simeq 0.577216$ is Euler's constant, one can determine the radius of influence, R_∞, of the pumping well by considering a cone of depression centered about the well ($x_D = 1$) and defining R_∞ as

$$s_D|_{r_D = R_{D,\infty}} = 0 \tag{33}$$

This leads to

$$R_{D,\infty} = A t_D^{1/2} \tag{34a}$$

$$A = \sqrt{4\alpha} e^{-\gamma/4} \approx 1.73\sqrt{\alpha}. \tag{34b}$$

Then $L_D \approx R_{D,\infty}$ can be set when evaluating Equation (31).

2.3 Application to Field Observations

In this work, to test the hypothesis that streams respond to groundwater pumping, we observed the response of a stream-aquifer system to groundwater pumping for irrigation.. The null hypothesis in this case is that streams act as constant-head boundaries or as sources of the mass-transfer type with fixed stage, supplying recharge to an aquifer indefinitely during groundwater pumping. In the following, we provide evidence from field observations that a stream in hydraulic contact with a pumped aquifer experiences transient drawdown in response to the pumping. We also use the newly developed flow model and the field observations of stream drawdown, in addition to aquifer drawdown data, to estimate aquifer hydraulic properties, stream conductance, and the newly introduced finite stream storage coefficient C_r.

2.3.1 Study Site Description

The study site is situated in the agricultural fields of the California Polytechnic State University (Cal Poly), San Luis Obispo, located along the California central coast. The site is an alluvial basin underlain with a shallow confined aquifer of gravel and sand, which underlain with low permeability metavolcanic bedrock. The site is situated at the northern edge of the greater San Luis Obispo aquifer where the water-bearing geologic formations comprise recent (Quaternary) alluvium, Paso Robles Formation, and Pismo Formation. The metavolcanic bedrock is locally interpreted to belong to the non-water-bearing Franciscan assemblage. The groundwater basin in which the aquifer is situated has been designated as medium priority in the implementation of the Sustainable Groundwater Management Act (SGMA) passed in the state of California in 2014. Hence, the modeling, data, and results presented here have great implications for an aquifer of societal relevance.

The aquifer is bounded above by a thin near-surface layer of variably saturated clay or clay-rich sediment of very low permeability. This layer constitutes the upper confining unit (upper aquitard) and has a thickness of 13 m. The aquifer is confined from below at a depth of about 24 m by metavolcanic bedrock. The aquifer has an average thickness of approximately $b = 11$ m locally as determined from drilling logs for well installation. A stream, Stenner Creek, flows across the study site on top of the aquifer in a nearly northwest-to-southeast direction, incising through the entire thickness of the confining layer overlying the aquifer. As will become clear in the following, the stream is in direct hydraulic contact with the aquifer. The

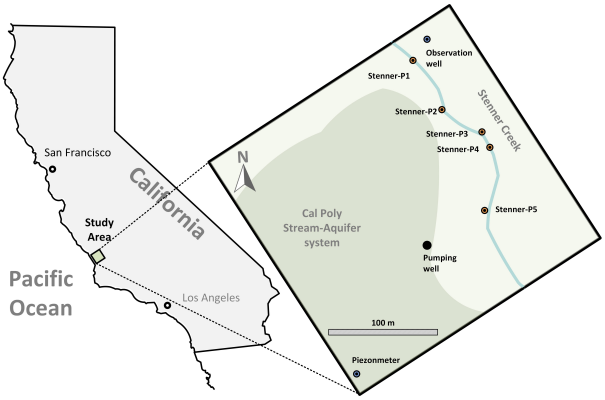

Figure 2. The map of the study site at California Polytechnic State University, San Luis Obispo, showing the observation locations along the stream and the observation well and the aquifer piezometer.

streambed is of the same sand and gravel formation as the aquifer, and the stream has minimal penetration of the aquifer. During the summer low flows, the discharge rate of the stream is on the order of $Q_s \sim 5 \times 10^{-4}\ \mathrm{m}^3/\mathrm{s}$.

2.3.2 Monitoring of Aquifer Pumping

An irrigation well, which serves as the pumping well in this study, has a diameter of about 0.2 m and is located about 60 m southwest of the stream, as depicted in Figure 2. It is completed throughout the thickness of the aquifer and is used to pump confined aquifer regularly on a fortnightly schedule at a constant rate of $Q = 8.58 \times 10^{-3}\ \mathrm{m}^3/\mathrm{s}$. Aquifer drawdown response to pumping was continuously monitored with transducers in the pumping well and a nearby abandoned well located across the stream about 10 m from the bank as shown on the map. A piezometer situated about 100 m due west of the pumping well was also instrumented for monitoring aquifer response. It is completed in the top 1 m of the aquifer just below the overlying confining unit. To monitor the stream stage, pressure transducers (Stenner-P1, P2, and P3) were placed in the stream channel in stilling wells without penetrating the streambed at three locations. Two additional stream channel monitoring stations downstream of Stenner-P3 were instrumented with pressure transmitters connected to CR300 data loggers (Campbell Scientific, Inc.) and are marked Stenner-P4 and P5 on the site map in Figure 2. Stream stage was continuously monitored at 15-minute intervals at these five locations.

Drawdown data were obtained by denoising and detrending the raw time series data shown in the figure. The raw data were denoised using singular spectrum analysis and detrended using the ensemble empirical mode decomposition method to remove unfavorable noises arising from the diurnal evapotranspiration signal of the riparian corridor and the trend due to rainfall events (highlighted in blue in the figure). These functions can be found in the built-in functions in the Python package called pyts.decomposition (Johann, 2021) and PyEMD (Laszuk, 2020), respectively. Six pumping events recorded during the spring and summer irrigation seasons of 2022 are highlighted gray in the figure. Due to instrument malfunction, not all episodes

of pumping were recorded by each of the monitoring stations. The six pumping events analysed in this work occurred on March 16 starting at 9:35, April 27 at 7:12, May 31 at 13:53, June 23 at 9:30, July 18 at 12:05, and August 8 at 7:22 in 2022.

2.3.3 Drawdown Analysis and Parameter Estimation

To demonstrate the applicability of the model to field observations of stream and aquifer drawdown, a model fitting and parameter estimation exercise was conducted using observed drawdown. Based on the configuration of the stream and aquifer at the study site, the NPS solution was used to identify the hydraulic parameters of the aquifer, namely, K_x, κ, and S_s, as well as the streambed conductance, β, and the stream channel storage coefficient, C_r. The solution proposed in this study was coupled with the Levenberg-Marquardt optimization algorithm as implemented in MATLAB. The purpose of the exercise was to identify parameter values that minimize the sum of the residuals between the observed and model predicted drawdown as expressed in the objective function

$$F(Y) = \sum_{n=1}^{N} \left[s_{\text{obs},}(x, y, t_n) - s(x, y, t_n; Y) \right]^2 \tag{35}$$

where N is the total number of temporal drawdown observations, $s_{\text{obs}}(x, y, t_n)$, at location (x, y) at time t_n, and $s(x, y, t_n; Y)$ are the corresponding model computed values given the set of parameters $Y = \{K_x, S_s, \kappa, \beta, C_r\}$. The convergence criterion for the optimization process was set to $F(Y_{\text{opt}}) < 1 \times 10^{-4}$, where Y_{opt} is the set of parameters that minimizes the objective function in equation (35). The hydraulic parameters were log-transformed to constrain the optimization procedure to the positive space of the parameter values.

Additionally, estimated values of hydraulic parameters were checked against published values of geologic materials with similar sediment composition to ensure reliability. The aquifer at the study site is predominantly sand and gravel; therefore, the reasonable range for hydraulic conductivity is $K_x \in \left[10^{-6}, 10^{-3}\right]$ m/s, with $K_y = \kappa K_x$ where $\kappa \sim 1.0$. The typical range for specific storage is $S_s \in \left[10^{-6}, 10^{-3}\right]$ m^{-1}, and $\beta > 10^{-9}$ s^{-1}. The value of C_r is bounded only by the log-transformation during the parameter estimation procedure; no published values are available in the hydrogeology literature because the parameter was first introduced in this work. It is expected, however, that this parameter would generally be greater than storativity, $S = bS_s$.

In this work, parameter estimation is conducted by considering only drawdown data from the aquifer observation well and the stream stilling well Stenner-P1. The pumping well is located at $R = 62.2$ m and has x-y coordinates $(62.2, 0.0)$ m. The stream observation location Stenner-P1 is located in the middle of the stream channel at $(-0.75, 183.1)$ m, whereas the observation well location is on the far-side of the stream at $(-15.1, 193.6)$ m. The stream channel had an average width of about $w = 1.5$ m during the Spring-Fall period of 2022 when the data analysed here were collected. The aquifer has an average thickness of 11 m, estimated from drilling logs of the pumping and irrigation wells. In all the tests analysed here, groundwater was pumped at a constant rate of $Q = 135$ gallons per minute (gpm) to irrigate one half of a lemon orchard for 24 hours, and the other half for another 24-hour period for a total of 48 hours of pumping. However, the pumping rate increases slightly to about 138 gpm at the start of the second 24-hour irrigation period, which has the effect of changing the trajectory of transient

drawdown response. Hence, for this work, only data from the first 24 hours (1440 min) of pumping are analysed for the purpose of parameter estimation. Recovery phase data are not considered here in order to simplify the analysis.

3 Results

The results presented here are separated into three parts, namely (1) the model predicted behavior, (2) the observed drawdown response of the stream and aquifer at the study site, and (3) estimation of aquifer hydraulic parameters by fitting the model to observed aquifer and stream drawdown.

3.1 Model Predicted Aquifer and Stream Drawdown

Transient aquifer and stream drawdown predicted by the developed herein are shown in Figure 3, where the graph in (a) shows the behavior predicted by the NPS model, and (b) that predicted by the FPS model. The graphs are plots of dimensionless drawdown on the vertical axis versus dimensionless time, t_D/r_D^2, on the horizontal axis. The model predicted behavior is plotted with the limiting cases of Theis (1935), Ferris et al. (1962), Hantush (1965), and Fox et al. (2002) for comparison. The models of Hantush (1965) and Fox et al. (2002) correspond to the limiting case of infinite stream channel storage ($C_r \to \infty$) for the NPS and FPS models, respectively. The model of Theis (1935) is shown in Figure 3(a) as the limiting case of $C_r = 0$ for the NPS solution for an impermeable barrier at the stream-aquifer interface when there is no water in the stream, while that of Ferris et al. (1962) is included in (b) for the FPS case.

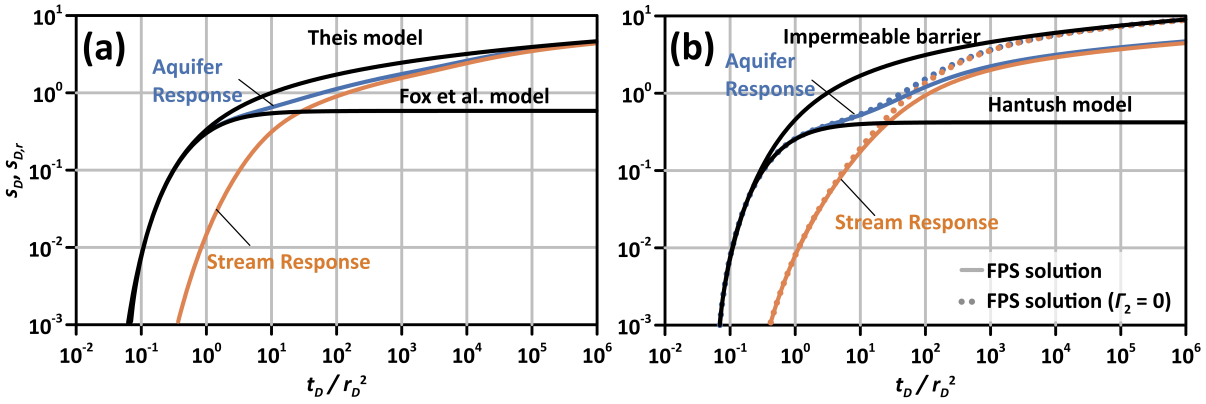

Figure 3. Transient aquifer and stream drawdown response predicted by the (a) NPS and (b) FPS solutions. The limiting cases of Theis (1935), Fox et al. (2002), Ferris et al. (1962), and Hantush (1965) are included for comparison.

The dependence of the model predicted temporal behavior of aquifer and stream drawdown on the dimensionless stream channel storage coefficient, $C_{D,r}$, is depicted in Figure 4. The models of Fox et al. (2002) and Hantush (1965) are again included for comparison. In the figure, the graphs (a) and (b) show, respectively, the NPS and FPS solutions on the pumped

half-space at $(x, y) = (0.5, 0)$, while graphs (c) and (d) show the corresponding predicted behavior in the unpumped half-space at $(x, y) = (-1.5, 0)$.

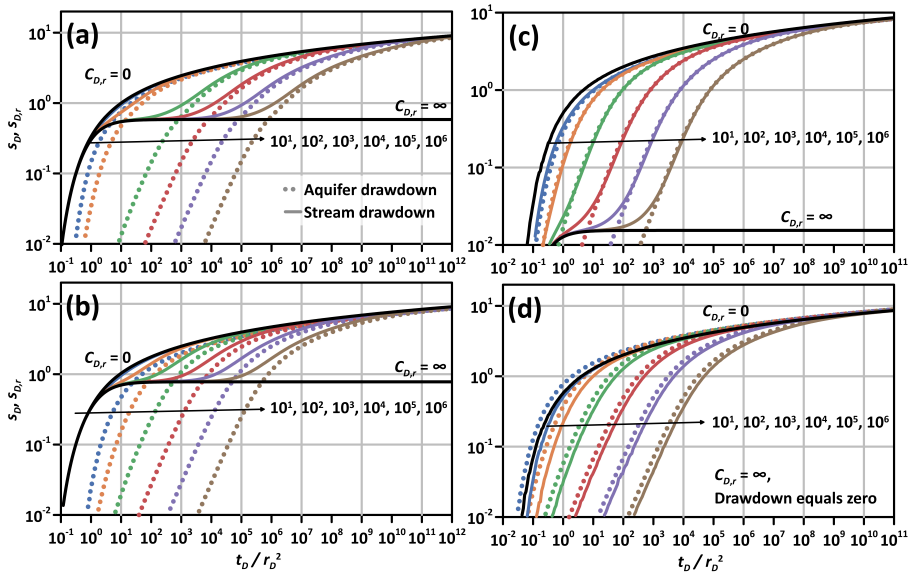

Figure 4. Model predicted temporal behavior of aquifer and stream drawdown for different values of $C_{D,r}$ ranging from 10 to ∞. Graphs (a) and (b) show, respectively, the NPS and FPS solutions on the pumped half-space at $(x, y) = (0.5, 0)$. Graphs (c) and (d) show the corresponding response in the unpumped half-space at $(x, y) = (-1.5, 0)$.

The effect of dimensionless streambed conductance, β_D, on aquifer and stream drawdown is depicted in Figure 5. The curves in the graphs are for different values of β_D ranging from an impermeable streambed at $\beta_D = 0$ to a highly conductive one at $\beta_D = 10$. The results are shown for both the pumped (a and b) and the unpumped (c and d) half-spaces of the respective flow domain.

Drawdown derivative analysis is a useful tool to diagnose the change in flow behavior because it can markedly improve the sensitivity of the model behavior to hydraulic parameters leading to improved parameter identifiability (Bourdet et al., 1983; Chow, 1952; Ferroud et al., 2018, 2019). Figure 6 shows the temporal behavior of aquifer and stream drawdown time derivatives and their dependence on $C_{D,r}$. The graphs show the derivative plots of the two solutions in the pumped half-space(a and b) at (0.5, 0) and in the stream (c and d) at (-0.5, 0). The different curves are obtained by varying the values of $C_{D,r}$ from 1 to 10^9. The graphs are plots of $\partial s_D / \partial \ln(t_D)$ for the aquifer flow response or $\partial s_{D,r} / \partial \ln(t_D)$ for the flow response of the stream. Figure 7 shows the dependence of the same temporal derivatives on dimensionless streambed conductance, β_D, over the range 0 to 10^5.

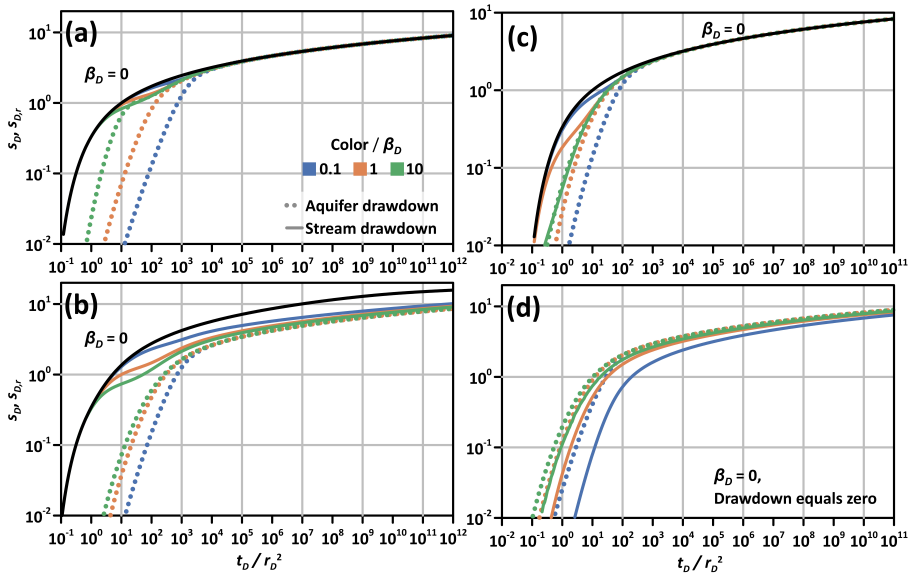

Figure 5. Model predicted temporal behavior of aquifer and stream drawdown for different values of β_D ranging from 0 to 10. Graphs (a) and (b) show the NPS and FPS solutions on the pumped half-space, while (c) and (d) are corresponding solution in unpumped half-space).

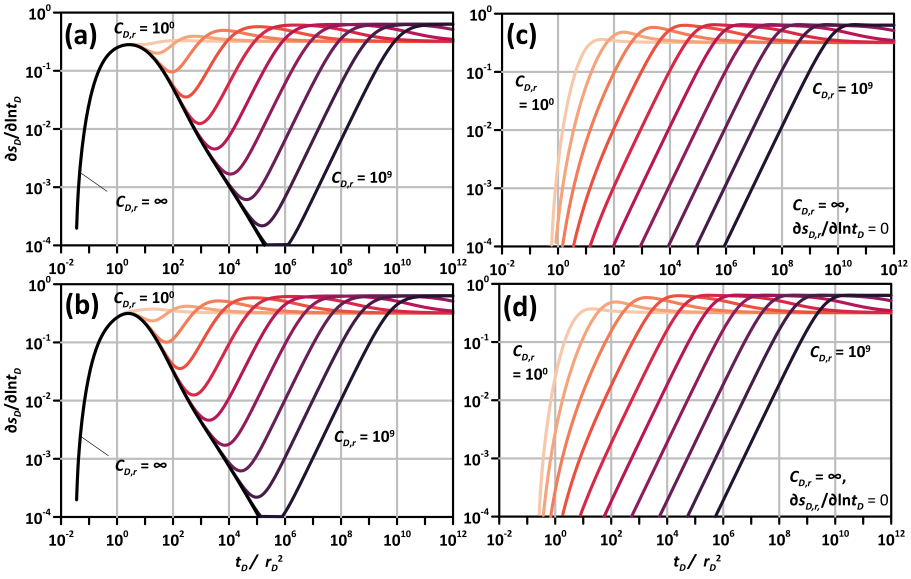

Figure 6. Temporal aquifer drawdown derivatives for the cases of (a) NPS and (b) FPS solutions and stream derivatives for the cases of (c) NPS and (d) FPS solutions with varying $C_{D,r}$ values from 1 to ∞.

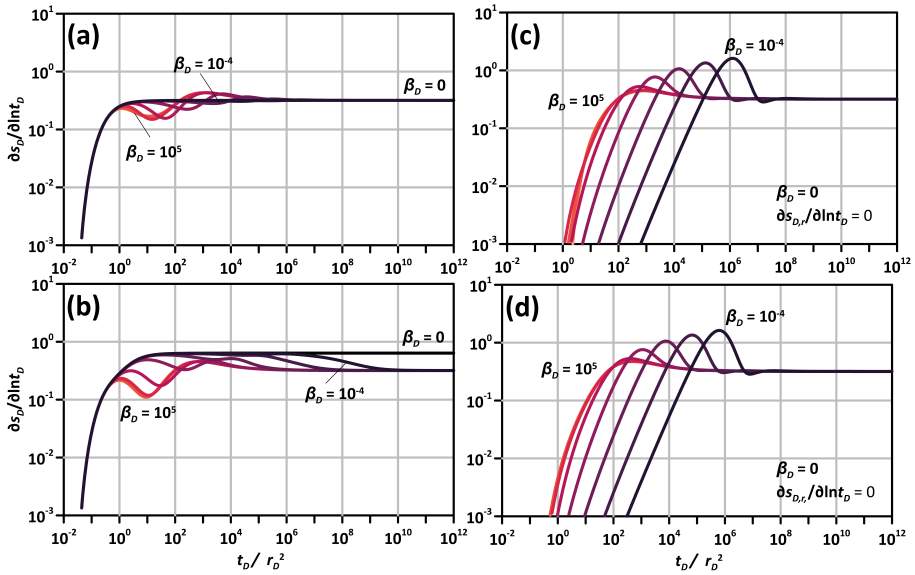

Figure 7. Temporal aquifer drawdown derivatives for the cases of (a) NPS and (b) FPS solutions and stream derivatives for the cases of (c) NPS and (d) FPS solutions with varying β_D values from 0 to 10^5.

3.2 Model Predicted Stream Depletion

The predicted stream depletion rate (SDR), $Q_{D,r}$, is illustrated in Figure 8, where we explore the effect of $C_{D,r}$ on the $Q_{D,r}$ predicted by (a) NPS solution, (b) FPS solution, and (c) FPS solution with $\Gamma_2 = 0$. The Figure also shows the effect of β_D on the behavior of $Q_{D,r}$ predicted by the models.

3.3 Observed Transient Aquifer and Stream Drawdown

The time series (hydrographs) of the aquifer water levels in an observation wells and piezometer as well as stream stage at the four monitoring locations, relative to the long-term background levels, are plotted in Figure 9. Aquifer drawdown obtained data by detrending and denoising observation well water levels are shown in Figure 10 for the six tests highlighted previously. The figure shows (a) log-log and (b) semi-log plots of the observed drawdown. The figure also shows in (c) the log-time derivative of the drawdown data computed numerically using central differences. The recovery data are also included for completeness.

Observed stream stage drawdown data are shown in Figure 11 for the four monitoring stations. The response of the aquifer in test 6 is also included in all the graphs for comparison. The data are plotted on log-log scale for (a) Stenner P1, (b) Stenner P2, (c) Stenner P3, and (d) Stenner P5, with elapsed time since onset of pumping on the horizontal axis and drawdown on the vertical axis.

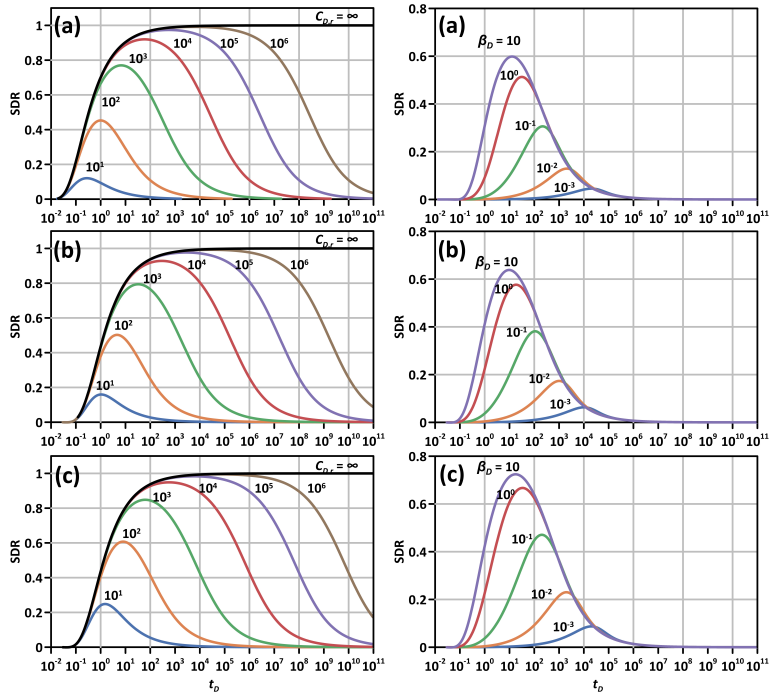

Figure 8. Temporal SDR for different (left column) $C_{D,r}$ values from 10 to ∞ and for different (right column) β_D values from 10^{-3} to 10 predicted by (a) the NPS solution, (b) FPS solution, and (c) FPS solution with $\Gamma_2 = 0$.

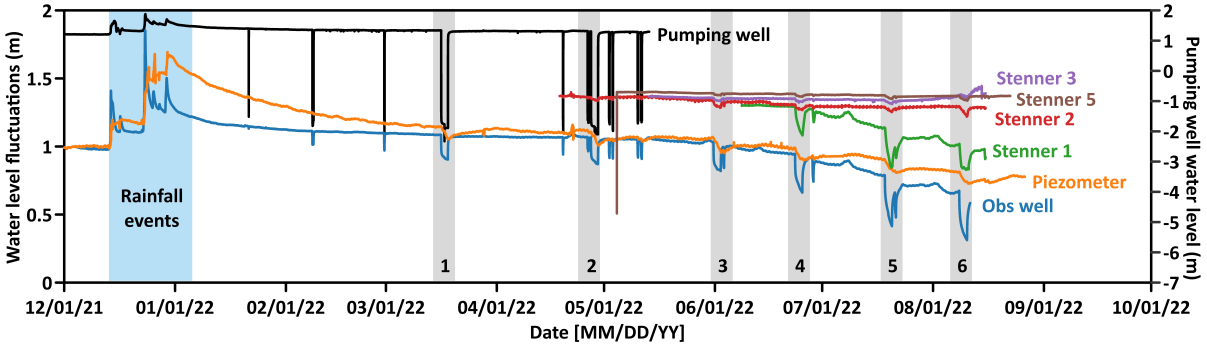

Figure 9. Time series of groundwater and stream stage fluctuations observed in the stream-aquifer system. The six pumping events are colored gray and labeled 1-6. All data are plotted on vertical axis on the left except pumping well water levels, which are on the right axis.

3.4 Analysis of Aquifer and Stream Drawdown

The results of model fits to the data and the corresponding parameter estimation exercise are shown in Figure 12. The best model fits of the NPS model to the observation well (aquifer) drawdown data for the six tests highlighted above are plotted

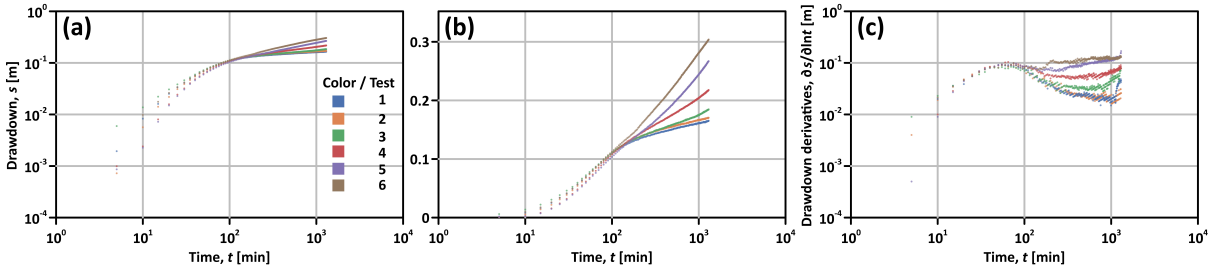

Figure 10. Plots of aquifer drawdown recorded in the observation well from six pumping tests on the (a) log-log and (b) semi-log scale. The logarithmic time derivative of drawdown is plotted in (c) using centered differencing.

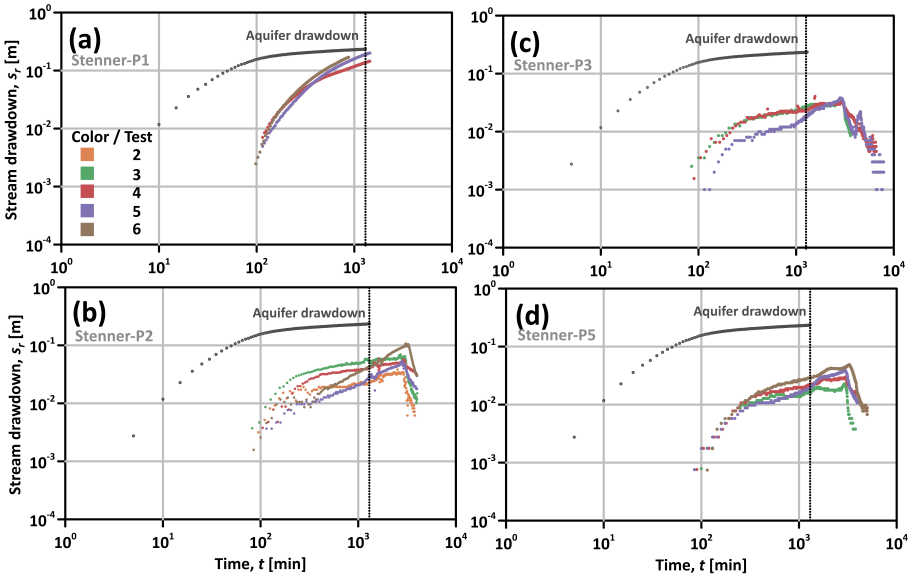

Figure 11. Log-log plots of transient stream stage drawdown response to pumping observed in stream channel stilling wells (a) Stenner-P1, (b) Stenner-P2, (c) Stenner-P3, and (d) Stenner-P5. The data also show stage recovery after pumping (dashed lines for pumping after 48 hrs). Aquifer response (gray dots) is included for comparison.

on (a) log-log, (b) semi-log, and (c) linear scales. The corresponding estimated parameter values for the model fits to data that minimize the objective function defined previously are summarized in Table 3. All the model fits to the aquifer drawdown data were obtained with values of $K_x = 8.31 \times 10^{-5}$ m/s for hydraulic conductivity and $S_s = 1.46 \times 10^{-5}$ m^{-1} for specific storage. These values were obtained with test 6 data and then held fixed in the subsequent analyses. Only parameters κ, β, and C_r were allowed to vary among all the subsequent analyses of tests 1-5.

Figure 12 also includes (in d, e, and f) the predicted stream drawdown behavior at Stenner-P1 using the parameter values in Table 3 from analysis of aquifer drawdown. Given the model-data misfit, stream drawdown data were used to independently fit

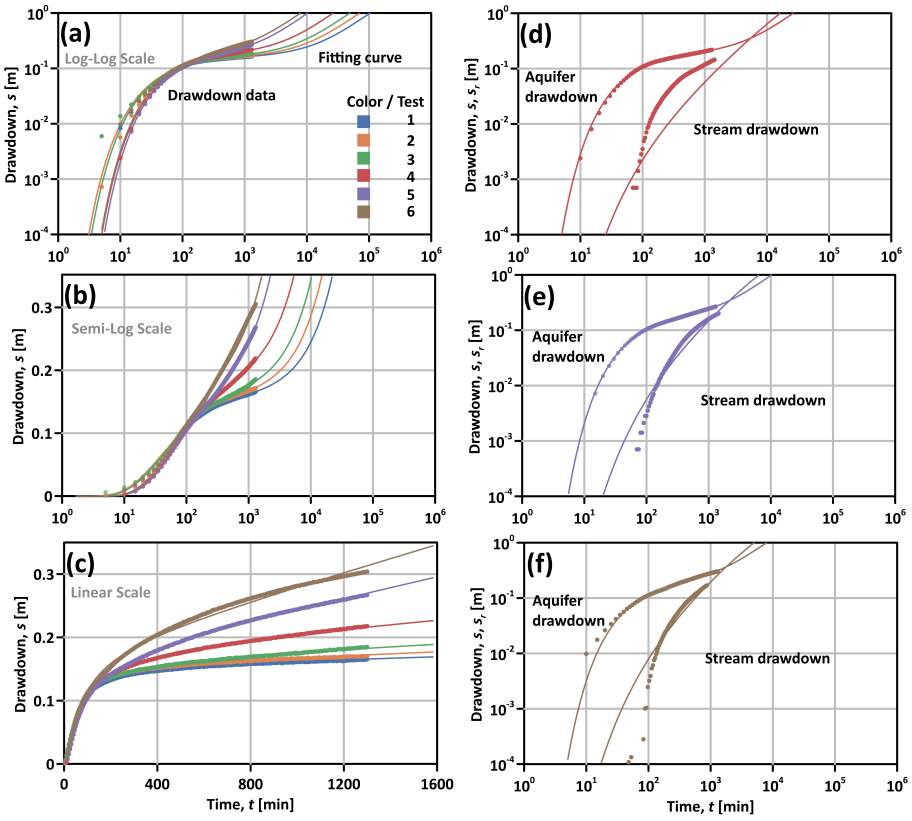

Figure 12. Results of transient analysis of aquifer drawdown response from individual tests showing model fits to observation well data in (a) log-log scale, (b) semi-log scale, and (c) in linear scale. Model predicted stream drawdown response is compared to observations in (d), (e), and (f) using parameters estimated from aquifer data.

Table 3. Estimated parameter values using aquifer drawdown data from the observation well.

Test	K_x (m/s)	κ (-)	S_s (1/m)	β (1/s)	C_r (-)
1	8.31×10^{-5}	0.591	1.46×10^{-5}	4.14×10^{-5}	68.0
2	8.31×10^{-5}	0.591	1.46×10^{-5}	4.09×10^{-5}	46.1
3	8.31×10^{-5}	0.674	1.46×10^{-5}	4.02×10^{-5}	33.2
4	8.31×10^{-5}	0.978	1.46×10^{-5}	3.56×10^{-5}	19.0
5	8.31×10^{-5}	1.09	1.46×10^{-5}	3.54×10^{-5}	7.09
6	8.31×10^{-5}	1.08	1.46×10^{-5}	3.49×10^{-5}	5.54
average	8.31×10^{-5}	0.836	1.46×10^{-5}	3.81×10^{-5}	29.8

Table 4. Estimated parameter values using NPS solution for the three recorded tests in the Stenner-P1. Parameters κ and β were fixed to values estimated with aquifer observation well drawdown data.

Test	K_x (m/s)	κ (-)	S_s (1/m)	β (1/s)	C_r (-)
4	8.88×10^{-4}	1.0	6.33×10^{-4}	1.03×10^{-4}	0.166
5	5.14×10^{-4}	1.0	5.19×10^{-4}	1.03×10^{-4}	0.447
6	3.92×10^{-4}	1.0	5.22×10^{-4}	1.03×10^{-4}	0.180

the model and estimate system hydraulic parameters. The resulting model fits to stream drawdown data at observation location Stenner-P1 are shown in Figure 13. The estimated parameter values are summarized in Table 4.

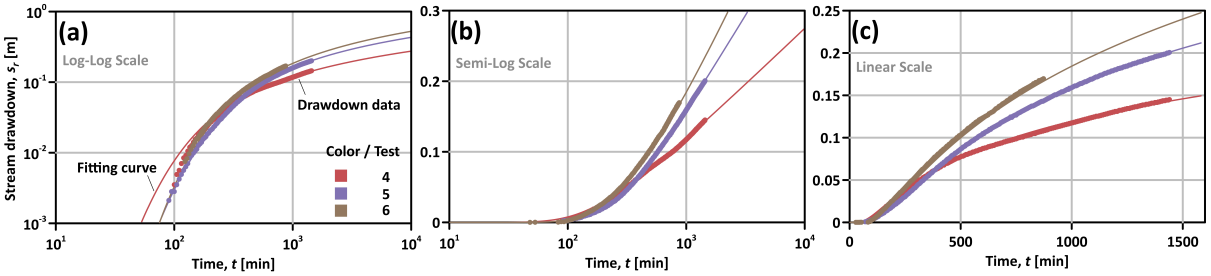

Figure 13. Results of transient analysis of stream drawdown response from individual tests showing model fits to the data for Stenner Creek stilling well S1. The results are plotted on (a) log-log, (b) semi-log, and (c) linear scales.

Figure 14 shows the change in the parameter values of C_r over the course of the six pumping tests. For each individual test, C_r was taken to be constant, but there was clear and consistent decrease from test 1 to 6.

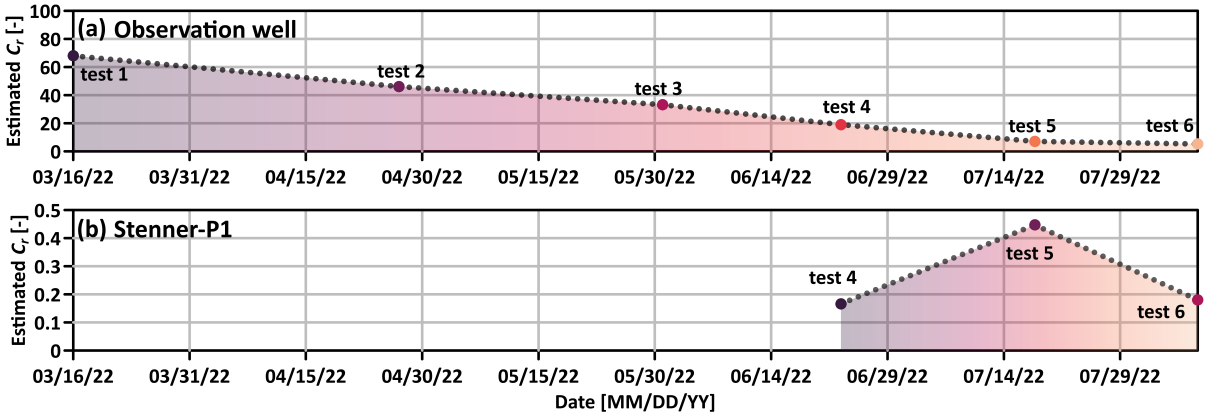

Figure 14. Time series of C_r estimated from the (a) observation well and (b) Stenner-P1 from six pumping tests.

4 Discussion

The predicted aquifer drawdown response shown in Figure 3 is characterized by three phases that are commonly observed in dual-storage media such as unconfined aquifers (Neuman, 1974; Malama, 2011; Mishra and Neuman, 2010; Lin et al., 2019) and dual-porosity fractured formations (Warren and Root, 1963; Streltsova, 1983; De Smedt, 2011; Lin and Yeh, 2021). The three phases predicted by the present model are termed here as early-, intermediate-, and late-time. During early-time, aquifer response follows the limiting models of Theis (1935) and Ferris et al. (1962) for the NPS and FPS models, respectively, which corresponding to $C_{D,r} \equiv 0$. Stream drawdown response is virtually imperceptible during this early-time phase as water flows primarily from aquifer elastic storage. The onset of intermediate-time is marked by significant departure of aquifer drawdown from limiting case of $C_{D,r} \equiv 0$ transitioning to closely follow the behavior predicted by the limiting solutions of Fox et al. (2002) and Hantush (1965) for $C_{D,r} \to \infty$. During this transition period, stream appears to initially serve as a near-infinite store of water and aquifer drawdown appears to approach steady-state. For finite values of $C_{D,r}$, this "steady-state" phase is only momentary as aquifer drawdown begins to increase again and stream stage begins to respond to pumping. If pumping were to cease during the early part of intermediate-time, the models of Fox et al. (2002) and Hantush (1965) would be sufficient to describe system behavior. The higher stream storage coefficient, $C_{D,r}$, the longer this quasi-static phase persists. As pumping continues, the aquifer drawdown response transitions into late-time transient behavior characterized by increasing aquifer drawdown response, which rises above the steady-state values predicted by the fixed-stage models of Fox et al. (2002) and Hantush (1965). This suggests that these models underestimate aquifer drawdown at late-time. At very late-time, aquifer drawdown transitions into the behavior predicted by models with a no-flow condition at the tream-aquifer interface.

The results indicate that stream stage drawdown response is delayed relative to aquifer drawdown, and only appears to start during the late-time phase. It is shown to exceed the late-time steady-state aquifer drawdown predicted by the fixed-stage models of Fox et al. (2002) and Hantush (1965). Depending on the initial stage of the stream, stream drawdown would lead to drying up of streams at very late-time, during prolonged periods of groundwater pumping.

Model results shown in Figure 4 indicate that increasing the values of $C_{D,r}$ has the effect of prolonging the intermediate phase and increasing the delay in stream stage drawdown response to pumping. Deep streams with high discharge may be associated with high values of channel storage, and would require prolonged pumping at high rates to induce stream drawdown. This may take several days, which explains why such streams are typically treated as fixed-stage boundaries. Model results in Figure 5 suggest that stream stage responsiveness to pumping increases with increasing values of β_D, leading to decreasing lag times between stream and aquifer drawdown responses.

Results of drawdown derivative analysis shown in Figure 6 indicate that for the case of $C_{D,r} = \infty$, the drawdown derivative is characterized by values that initially rise steeply, reaching a peak value before declining down to vanishingly small values. This is a typical feature of a fixed-head recharge boundary effect Ferroud et al. (2019) where aquifer drawdown behavior attains to a steady state. However, for finite values of $C_{D,r}$, the drawdown derivative displays a double hump with an initial peak associated with transition from early- to intermediate-time drawdown behavior and a second peak associated with transition from intermediate- to late-time behavior. The second peak is typically higher that the first one and is subsequently

followed by a late-time derivative derivative decline a constant value. Between the two peak values is a unique minimum for each value of $C_{D,r}$. The times at which these unique minima of the derivatives of aquifer drawdown occur appear to represent the starting time of the stream drawdown response. The valley pattern of the aquifer drawdown derivative is typical of storage porosity systems, and in this case, it represents the transition between discharge of water from elastic storage to that from stream storage. The stream drawdown derivative increases to a single peak value before gradually decline until it returns to a constant level. The peak value generally coincides in time with the second peak of the aquifer drawdown derivatives. The behavior of the derivative of aquifer drawdown appears to be less sensitive to the dimensionless streambed conductance, β_D, but the features of the curves may still be useful in identifying the streambed conductance from stream drawdown data.

The results in Figure 8 show that, generally, for finite values of $C_{D,r}$, the depletion rate, $Q_{D,r}$, increases initially with time before reaching a peak rate followed by a subsequent decline. In this instance, the solution of Zlotnik (2004) serves as the limiting case of depletion rate. The behavior of $Q_{D,r}$ for finite values of $C_{D,r}$ differs significantly from that predicted for $C_{D,r} \to \infty$ where the maximum depletion rate stays fixed at $Q_{D,r} = 1.0$ indefinitely, with all water captured by the pumping well at late-time coming from stream recharge. For finite values of $C_{D,r}$, the depletion rate reaches a peak value of $Q_{D,r} \leq 1.0$, with a unimodal distribution pattern, indicating that the peak depletion rate is only a fraction of the pumping rate even at late-time, with the rest of the water coming from aquifer storage, as stream stage declines and the stream approaches dryness. As $C_{D,r}$ increases, the stream contributes increasing proportions of the water abstracted by the pumping well at late-time and the curves of $Q_{D,r}$ are closer to the limiting case of $C_{D,r} \to \infty$. The results in Figure 8 also show that $Q_{D,r}$ increases with increasing β_D because higher values of β_D are associated with a higher degree of stream-aquifer connectivity. Increasing values β_D have the effect of shifting the $Q_{D,r}$ peaks leftward to earlier times and upward to greater peak depletion rates.

Analysis of drawdown data from the observation well show a general shift in aquifer drawdown behavior over the course of the six pumping events during the summer 2022 irrigation season. The least overall drawdowns were recorded in the first of the pumping periods of March 16 to March 18, while the largest were recorded in the last reported pumping period. This behavior is reflective of the decrease in the amount of water stored in the stream channel (C_r) from the spring high flows to the summer lows. However, for any given test, C_r may be treated as a constant and the observed transient aquifer response generally shows the three phases predicted by the model developed in this work, namely early-, intermediate-, and late-time behavior. These phases are most evident in the latter tests (4,5,6) that are associated with small values of the parameter C_r. The earlier tests (1,2,3), when the stream channel has the most water (large C_r) primarily show the early- and intermediate phases as the stream acts more like a fixed-stage boundary. Even for the earlier tests, the intermediate phase does not attain to late-time drawdown steady state predicted by the fixed-stage models of Hantush and Jacob (1955) and Fox et al. (2002).

Another important observation of note is that a nonzero, coherent, and unambiguous transient stream drawdown response is clearly evident in the data. For the present study site, the stream clearly does not behave as having a fixed-stage, supplying recharge indefinitely. Additionally, the observed stream drawdown response at all measuring locations is significantly delayed relative to aquifer drawdown. All the stream stage observation locations are located closer to the pumping well than the aquifer observation well but all start showing measurable drawdown response at much later times (over an hour later) than the aquifer observation well. This delayed stream response confirms a key model prediction shown in Figure 3.

Results of the model fit exercise based on aquifer drawdown data shown in Figure 12 demonstrate that excellent model fits to data are obtainable with $R^2 \geq 95\%$. The associated parameter values estimated from the data and summarized in Table 3 clearly demonstrate that reasonable aquifer hydraulic parameters as well as streambed conductance and stream channel storage values are obtainable with the model developed in this work from the observed aquifer drawdown response. It is, however, clear that the stream drawdown behavior predicted on the basis of hydraulic parameters estimated with aquifer drawdown only deviates significantly from the observed behavior at Stenner-P1. This is particularly the case for test 4 data depicted in Figure 12(d). Hence, stream drawdown data where analysed separately and the resulting model fits to observed transient behavior are shown in Figure 13. The model fits to stream drawdown data show a marked improvement and the resulting parameter values are summarized in Table 4. These values are appreciably different from those estimated from aquifer drawdown data (see Table 3), which may be attributed to aquifer and streambed heterogeneity. This discrepancy in model parameters estimated from stream versus aquifer drawdown data may highlight a deficiency in the theory developed here where stream flow velocity is neglected in the stream channel mass balance condition. For the present case, it is sufficient to demonstrate that the hydraulic parameters of the system are estimable from the data.

In the analysis of aquifer drawdown data, the most significant parameter change among the 6 tests was observed in the stream storage coefficient C_r. The results are plotted in Figure 14, showing the change in the value of C_r over the course of the six pumping tests. For each individual test, C_r was taken to be constant, but there was clear and consistent decrease from test 1 to 6 over the irrigation season from March to August 2022. This decrease of C_r over the course of the pumping season correlates with a reduction in stream stage and discharge during the dry season. This variation notwithstanding, the results, indicate that the stream storage is finite and estimable and may be treated as fixed only for a relatively short duration corresponding to a single pumping event.

5 Conclusions

The modeling and data analysis results presented in this work demonstrate that aquifer flow models with a fixed stream stage boundary condition or source term underestimate aquifer drawdown and overestimate the capacity of a stream to buffer aquifer drawdown through continuous recharge. It is demonstrated here that streams may have finite and estimable channel storage and that can undergo both depletion and drawdown in response to groundwater pumping from a hydraulically connected aquifer. This is especially critical in aquifer systems subjected to prolonged groundwater abstraction, which can lead to the drying of streambeds, as has been observed in many groundwater basins with irrigated agriculture. Models with fixed stream stage overestimate the available groundwater supply from the stream because of their inherent assumption of infinite stream storage. The results of this work have implications for sustainable groundwater management. The model developed may be used to not only predict the stream depletion rate but also the decline of stream stage. Additional work is needed to incorporate stream discharge (or velocity) in the model and to conduct longer pumping tests than reported herein in order to better constrain parameter estimates. This may resolve the discrepancy in model parameter values estimated from independent analyses of aquifer and stream drawdown data.

Code and data availability. Mathematica and MATLAB codes developed for the study are available at the hyperlinks: HydroShare and MATLAB File Exchange. The raw data analyzed in this work are available from the corresponding author upon request.

Appendix A: Non-dimesionalization of NPS Flow Problem

On the basis of Table 2, the governing equation, in dimensionless form, for the case of NPS, is as follows.

$$\frac{\partial s_D}{\partial t_D} = \frac{\partial^2 s_D}{\partial x_D^2} + \kappa \frac{\partial^2 s_D}{\partial y_D^2} + f_{s,D}, \tag{A1}$$

where $s_{D,i} = s_{D,i}(x_D, y_D, t_D)$ is dimensionless aquifer drawdown, s_i/H_c, in the i^{th} sub-domain, with $i = 1,2,3$, $H_c = Q/(2\pi b K_x)$ is a system characteristic head, $x_D = x/R$ and $y_D = y/R$ are dimensionless distances in the x and y directions, $t_D = t/T_c$ is dimensionless time, $T_c = R^2/\alpha_x$ is a characteristic system time, $\alpha_x = K_x/S_s$ is aquifer horizontal hydraulic diffusivity in the x-direction, $\kappa = K_y/K_x$ is the anisotropy ratio in the horizontal plane, and $f_{s,D} = f_{s,D}(x_D, y_D, t_D)$ is the piecewise dimensionless sink/source term defined by

$$f_{s,D} = \begin{cases} -2\delta(x_D - 1)\delta(y_D) & x_D > 0, \\ \Gamma_D & x_D \in (-W_D, 0), \\ 0 & x_D \leq -W_D. \end{cases} \tag{A2}$$

Here $\Gamma_D = \Gamma/[Q/(2\pi R^2)] = \beta_D(s_{D,2} - s_{D,r})$ is the dimensionless mass-transfer function at the stream-aquifer interface. A more complete list of dimensionless variables and relevant parameters is provided in Table 2. Equation (A1) is solved subject to the initial condition

$$s_D|_{t_D=0} = 0, \tag{A3}$$

and the far-field boundary conditions

$$\lim_{\substack{x_D \to \pm\infty \\ y_D \to \pm\infty}} s_D = 0. \tag{A4}$$

The dimensionless continuity conditions at $x_D = 0$ and $x_D = -W_D$ are specified as

$$s_{D,1}|_{x_D=0} = s_{D,2}|_{x_D=0}, \tag{A5}$$

$$s_{D,2}|_{x_D=-W_D} = s_{D,3}|_{x_D=-W_D}, \tag{A6}$$

for drawdown, and

$$\left.\frac{\partial s_{D,1}}{\partial x_D}\right|_{x_D=0} = \left.\frac{\partial s_{D,2}}{\partial x_D}\right|_{x_D=0} \tag{A7}$$

$$\left.\frac{\partial s_{D,2}}{\partial x}\right|_{x_D=-W_D} = \left.\frac{\partial s_{D,3}}{\partial x}\right|_{x_D=-W_D} \tag{A8}$$

for flux. In dimensionless form the stream-mass-balance condition becomes

$$C_{D,r}\frac{\partial s_{D,r}}{\partial t_D} = \beta_D(s_{D,2} - s_{D,r}), \tag{A9}$$

where $C_{D,r} = b_D C_r/S$ is the dimensionless stream storage coefficient, $s_{D,r} = s_r/H_c$, $\beta_D = \beta R/K_x$ is the dimensionless mass transfer coefficient across the streambed, $S = bS_s$ is aquifer storativity, and $b_D = b/R$ is dimensionless aquifer thickness. Note that C_r/S is simple the ratio of the stream storage coefficient to aquifer storativity. The dimensionless initial condition associated with this mass balance condition is

$$s_{D,r}(t_D = 0) = 0. \tag{A10}$$

Appendix B: Derivation of the NPS Solution

Applying the Laplace and Fourier cosine transforms to to equations A1 and A2 leads to

$$\eta^2\tilde{\tilde{s}}_D = \frac{\partial^2\tilde{\tilde{s}}_D}{\partial x_D^2} + \begin{cases} -\dfrac{2}{p}\delta(x_D - 1) & x_D > 0 \\ \pm\chi\tilde{\tilde{s}}_{D,2} & x_D \in (-W_D, 0) \\ 0 & x_D \le -W \end{cases}, \tag{B1}$$

where $\eta = \sqrt{p + \kappa\xi^2}$, $\chi = \beta_D p/(p + \beta_D^*)$, p is the Laplace transform parameter, and ξ is the Fourier cosine transform parameter. The problem domain in (x_D, y_D) dimensionless plane is symmetrical on either side of the x_D-axis; therefore, the problem domain $y_D \in (-\infty, \infty)$ can simply be reduced to $y_D \in [0, \infty)$. Therefore, the symmetric boundary conditions for s_D can be described by no-flow Neumann-type boundary conditions, i.e., $\partial s_D/\partial y_D$ at $y_D = 0$. The transformed governing equations for the NPS solution are

$$\eta^2\tilde{\tilde{s}}_{D,1} = \frac{\mathrm{d}^2\tilde{\tilde{s}}_{D,1}}{\mathrm{d}x_D^2} - \frac{2}{p}\delta(x_D - 1), \qquad x_D \in [0, \infty), y_D \in [0, \infty) \tag{B2}$$

$$\hat{\eta}^2\tilde{\tilde{s}}_{D,2} = \frac{\mathrm{d}^2\tilde{\tilde{s}}_{D,2}}{\mathrm{d}x_D^2}, \qquad x_D \in [-W_D, 0), y_D \in [0, \infty) \tag{B3}$$

$$\eta^2\tilde{\tilde{s}}_{D,3} = \frac{\mathrm{d}^2\tilde{\tilde{s}}_{D,3}}{\mathrm{d}x_D^2}, \qquad x_D \in (-\infty, -W_D), y_D \in [0, \infty) \tag{B4}$$

where $\hat{\eta}^2 = \eta^2 + \chi$.

The transformed dimensionless stream-mass-balance condition from equation (A9) is

$$p\tilde{\tilde{s}}_{D,r} = \beta_D^*(\tilde{\tilde{s}}_{D,2} - \tilde{\tilde{s}}_{D,r}), \tag{B5}$$

which can be rearranged as

$$\tilde{\tilde{s}}_{D,r} = \left(\frac{\beta_D^*}{p + \beta_D^*}\right)\tilde{\tilde{s}}_{D,2}. \tag{B6}$$

The far-field conditions are

$$\lim_{x_D \to \pm\infty} \tilde{\tilde{s}}_{D,1} = 0. \tag{B7}$$

The transformed continuity conditions from equations (A5) – (A7), respectively, are

$$\tilde{\tilde{s}}_{D,1}\big|_{x_D=0} = \tilde{\tilde{s}}_{D,2}\big|_{x_D=0}\,, \tag{B8}$$

$$\tilde{\tilde{s}}_{D,2}\big|_{x_D=-W_D} = \tilde{\tilde{s}}_{D,3}\big|_{x_D=-W_D}\,, \tag{B9}$$

$$\left.\frac{\mathrm{d}\tilde{\tilde{s}}_{D,1}}{\mathrm{d}x_D}\right|_{x_D=0} = \left.\frac{\mathrm{d}\tilde{\tilde{s}}_{D,2}}{\mathrm{d}x_D}\right|_{x_D=0}, \tag{B10}$$

$$\left.\frac{\mathrm{d}\tilde{\tilde{s}}_{D,2}}{\mathrm{d}x}\right|_{x_D=-W_D} = \left.\frac{\mathrm{d}\tilde{\tilde{s}}_{D,3}}{\mathrm{d}x}\right|_{x_D=-W_D}. \tag{B11}$$

Given the jump discontinuity introduced by the Dirac Delta source at $x_D = 1$, the solution for $\tilde{\tilde{s}}_{D,1}$ is piecewise, having the form

$$\tilde{\tilde{s}}_{D,1} = \begin{cases} A_1 e^{\eta x_D} + A_2 e^{-\eta x_D} & \forall x_D \in (1,\infty) \\ A_3 \cosh(\eta x_D) + A_4 \sinh(\eta x_D) & \forall x_D \in [0,1) \end{cases} \tag{B12}$$

where A_1 – A_4 are undetermined coefficients. From the farfield homogeneous boundary condition, it follows that $A_1 = 0$. The general solutions of equations (B3) and (B4) can be readily obtained and respectively give

$$\tilde{\tilde{s}}_{D,2} = A_5 \cosh(\hat{\eta} x_D) + A_6 \sinh(\hat{\eta} x_D) \tag{B13}$$

$$\tilde{\tilde{s}}_{D,3} = A_7 e^{\eta x_D} + A_8 e^{-\eta x_D} \tag{B14}$$

where A_5 to A_8 are coefficients to be determined by applying the boundary conditions defined above. From the farfield boundary conditions stated in equation (B7), the coefficients $A_8 \equiv 0$.

In addition to the boundary conditions already specified above, jump conditions across the Dirac Delta source at $x_D = 1$ are required to determine these coefficients. The jump conditions are

$$\tilde{\tilde{s}}_{D,1}\big|_{x_D=1^+} = \tilde{\tilde{s}}_{D,1}\big|_{x_D=1^-}\,, \tag{B15}$$

$$\left.\frac{\mathrm{d}\tilde{\tilde{s}}_{D,1}}{\mathrm{d}x_D}\right|_{x_D=1^+} = \left.\frac{\mathrm{d}\tilde{\tilde{s}}_{D,1}}{\mathrm{d}x_D}\right|_{x_D=1^-} - \frac{2}{p}, \tag{B16}$$

where $x_D = 1^{\pm} = \lim_{\delta \to 0} 1 \pm \delta$, where δ is a small interval across the Dirac Delta source. These two conditions enforce head or drawdown continuity at $x_D = 1$ and define the flux discontinuity, respectively. Applying these two conditions to the solution in Equation (B12) leads to

$$A_2 e^{-\eta} = A_3 \cosh(\eta) + A_4 \sinh(\eta), \text{ and} \tag{B17}$$

$$-A_2 e^{-\eta} = A_3 \sinh(\eta) + A_4 \cosh(\eta) - \frac{2}{p\eta}. \tag{B18}$$

Also, applying continuity conditions at $x_D = 0$ gives

$$A_3 = A_5, \text{ and} \tag{B19}$$

$$\eta A_4 = \phi A_6 = \hat{\eta} A_6. \tag{B20}$$

Finally, applying continuity conditions at $x_D = -W_D$ leads to

$$A_5 \cosh(\hat{\eta} W_D) - A_6 \sinh(\hat{\eta} W_D) = A_7 e^{-\eta W_D}, \text{ and} \tag{B21}$$

$$-A_5 \sinh(\hat{\eta} W_D) + A_6 \cosh(\hat{\eta} W_D) = \frac{\eta}{\hat{\eta}} A_7 e^{-\eta W_D}. \tag{B22}$$

Equations (B17)-(B22) fully define the linear system of equations needed to determine the coefficients A_2–A_7. These equations were solved in the Wolfram Mathematica environment and checked manually, yielding the coefficients as

$$A_2 = \frac{2}{p\eta}\left(\cosh(\eta) - \frac{\hat{\eta}}{\Delta_1} e^{-\eta} \hat{\chi}_2\right), \tag{B23}$$

$$A_3 = A_5 = \frac{2}{p\Delta_1} e^{-\eta} \hat{\chi}_1, \tag{B24}$$

$$A_4 = \frac{2\hat{\eta}}{p\eta\Delta_1} e^{-\eta} \hat{\chi}_2, \tag{B25}$$

$$A_6 = \frac{2}{p\Delta_1} e^{-\eta} \hat{\chi}_2, \text{ and} \tag{B26}$$

$$A_7 = \frac{2\hat{\eta}}{p\Delta_1} e^{-\eta(1-W_D)} \tag{B27}$$

where

$$\Delta_1 = 2\hat{\eta}\eta \cosh(\hat{\eta} W_D) + \left(\eta^2 + \hat{\eta}^2\right) \sinh(\hat{\eta} W_D), \tag{B28}$$

$$\hat{\chi}_1 = \hat{\eta} \cosh(\hat{\eta} W_D) + \eta \sinh(\hat{\eta} W_D), \text{ and} \tag{B29}$$

$$\hat{\chi}_2 = \eta \cosh(\hat{\eta} W_D) + \hat{\eta} \sinh(\hat{\eta} W_D). \tag{B30}$$

Substituting these coefficients into equations (B12) – (B14), the aquifer and stream drawdown solutions for NPS are obtained and shown in Equations (18) and (20), respectively.

Appendix C: Non-dimensionalization of FPS Flow Problem

The dimensionless governing equations for the FPS bounded by two aquifers are

$$\frac{\partial s_D}{\partial t_D} = \frac{\partial^2 s_D}{\partial x_D^2} + \kappa \frac{\partial^2 s_D}{\partial y_D^2} + f_D, \tag{C1}$$

with

$$f_D = \begin{cases} -2\delta(x_D - 1)\delta(y_D) & x_D > 0, \\ 0 & x_D < -W_D. \end{cases} \tag{C2}$$

Equation (C1) is solved subject to the dimensionless initial condition.

$$s_D|_{t_D=0} = 0, \tag{C3}$$

and far-field boundary condition

$$\lim_{\substack{x_D\to\pm\infty \\ y_D\to\pm\infty}} s_D = 0. \tag{C4}$$

The dimensionless flux boundary conditions at the stream-aquifer interfaces 1 and 2, respectively, are

$$\left.\frac{\partial s_{D,1}}{\partial x_D}\right|_{x_D=0} = \beta_D\left(s_{D,1}|_{x_D=0} - s_{D,r}\right), \tag{C5}$$

$$\left.\frac{\partial s_{D,2}}{\partial x_D}\right|_{x_D=-W_D} = \beta_D\left(s_{D,r} - s_{D,2}|_{x_D=-W_D}\right) \tag{C6}$$

The dimensionless stream-mass-balance condition becomes

$$C_{D,r}\frac{\partial s_{D,r}}{\partial t_D} = \beta_D\left(s_{D,1}|_{x_D=0} - s_{D,r}\right) + \beta_D\left(s_{D,r} - s_{D,2}|_{x_D=-W_D}\right). \tag{C7}$$

Equations (C1) – (C7) fully describe the well-posed nondimensional flow problem for a fully penetrating stream considered herein.

Appendix D: Derivation of the FPS Solution

The Fourier cosine transform method can then be used to eliminate y_D; meanwhile, the Laplace transform method can eliminate t_D in Equation (C1). The transformed flow equation for the pumped aquifer ($j = 1$) is

$$\eta^2\tilde{\bar{s}}_{D,1} + 2\delta_D(x_D - 1) = \frac{\mathrm{d}^2\tilde{\bar{s}}_{D,1}}{\mathrm{d}x_D^2}, \tag{D1}$$

for $x_D \in [0,\infty), y_D \in [0,\infty)$, and for the aquifer on the other side ($j = 2$) is

$$\eta^2\tilde{\bar{s}}_{D,2} = \frac{\mathrm{d}^2\tilde{\bar{s}}_{D,2}}{\mathrm{d}x_D^2}, \tag{D2}$$

for $x_D \in [-W_D,-\infty), y_D \in [0,\infty)$, where $\eta = \sqrt{p+\kappa\xi^2}$ with the Laplace parameter p and Fourier parameter ξ; the over-bar and tilde represent the function of the Laplace and Fourier domains, respectively.

Similarly, the dimensionless Laplace-Fourier-domain boundary conditions in x_D-direction are obtained as

$$\lim_{x_D\to\infty}\tilde{\bar{s}}_{D,1} = \lim_{x_D\to-\infty}\tilde{\bar{s}}_{D,2} \equiv 0. \tag{D3}$$

The dimensionless inner boundary conditions at $x_D = 0$ and $-W_D$, respectively, give the following.

$$\left.\frac{\mathrm{d}\tilde{\bar{s}}_{D,1}}{\mathrm{d}x_D}\right|_{x_D=0} = \beta_D(\tilde{\bar{s}}_{D,1} - \tilde{\bar{s}}_{D,r})|_{x_D=0}, \tag{D4}$$

$$\left.\frac{\mathrm{d}\tilde{\bar{s}}_{D,2}}{\mathrm{d}x_D}\right|_{x_D=-W_D} = \beta_D(\tilde{\bar{s}}_{D,r} - \tilde{\bar{s}}_{D,2})|_{x_D=-W_D}. \tag{D5}$$

The dimensionless stream mass-balance condition, equation (C7), in the Laplace-Fourier domain is

$$p\tilde{\bar{s}}_{D,r} = \beta_D^*(\tilde{\bar{s}}_{D,1}|_{x_D=0} - \tilde{\bar{s}}_{D,r}) - \beta_D^*(\tilde{\bar{s}}_{D,r} - \tilde{\bar{s}}_{D,2}|_{x_D=-W_D}). \tag{D6}$$

Rearranging equation (D6), one obtains

$$\tilde{\bar{s}}_{D,r} = \frac{\beta_D^*}{p+2\beta_D^*}(\tilde{\bar{s}}_{D,1}|_{x_D=0} + \tilde{\bar{s}}_{D,2}|_{x_D=-W_D}). \tag{D7}$$

The jump conditions at $x_D = 1$ are same as equations (D8) and (E7),

$$\tilde{\bar{s}}_{D,1}|_{x_D=1^+} = \tilde{\bar{s}}_{D,1}|_{x_D=1^-}, \tag{D8}$$

$$\left.\frac{\mathrm{d}\tilde{\bar{s}}_{D,1}}{\mathrm{d}x_D}\right|_{x_D=1^+} = \left.\frac{\mathrm{d}\tilde{\bar{s}}_{D,1}}{\mathrm{d}x_D}\right|_{x_D=1^-} - \frac{2}{p}. \tag{D9}$$

After applying the far-field boundary conditions, the solutions are

$$\tilde{\bar{s}}_{D,1} = \begin{cases} B_2 e^{-\eta x_D} & \forall x \geq 1, \\ B_3\cosh(\eta x_D) + B_4\sinh(\eta x_D) & \forall x \in [0,1] \end{cases} \tag{D10}$$

$$\tilde{\bar{s}}_{D,2} = B_5 e^{\eta x_D}\ \forall x_D < -W_D \tag{D11}$$

$$\tilde{\bar{s}}_{D,r} = \frac{\beta_D^*}{p+2\beta_D^*}(\tilde{\bar{s}}_{D,1}|_{x_D=0} + \tilde{\bar{s}}_{D,2}|_{x_D=-W_D})\ \forall x_D \in [-W_D, 0]. \tag{D12}$$

where B_2 – B_5 are undetermined coefficients. Upon applying the boundary and jump conditions, it can be shown that

$$B_2 = \frac{2}{p\Delta_2}\{\chi_1\cosh(\eta) + \chi_2\sinh(\eta)\} \tag{D13}$$

$$B_3 = \frac{2}{p\Delta_2}e^{-\eta}\chi_1 \tag{D14}$$

$$B_4 = \frac{2}{p\Delta_2}e^{-\eta}\chi_2 \tag{D15}$$

$$B_5 = \frac{2}{\Delta_2}\beta_D\beta_D^* e^{\eta(W_D-1)} \tag{D16}$$

where $\Delta_2 = p(\beta_D+\eta)\,[2\beta_D^*\eta + p(\beta_D+\eta)]$. Substituting these coefficients into Equations (D10) – (D12) leads to the solutions given in equations (21) and (26), for aquifer and stream drawdown.

Appendix E: Derivation of the FPS Solution for $\Gamma_2 = 0$

When $\Gamma_2 = 0$, the FPS solution will ignore the effect of unpumped aquifer. The same integral transformations applied previously are used. For the case for $\Gamma_2 = 0$, we only have to focus on solving the pumped aquifer, giving the following.

$$\eta^2\tilde{\bar{s}}_D + 2\delta_D(x_D - 1) = \frac{\mathrm{d}^2\tilde{\bar{s}}_D}{\mathrm{d}x_D^2}, \tag{E1}$$

for $x_D \in [0,\infty), y_D \in [0,\infty)$. We drop the subscript for drawdown because there is only one aquifer, that is, the pumped aquifer. The dimensionless Laplace-Fourier-domain boundary conditions in x_D-direction, are obtained as

$$\lim_{x_D \to \infty} \tilde{\tilde{s}}_D \equiv 0. \tag{E2}$$

$$\left.\frac{\mathrm{d}\tilde{\tilde{s}}_D}{\mathrm{d}x_D}\right|_{x_D=0} = \beta_D(\tilde{\tilde{s}}_D - \tilde{\tilde{s}}_{D,r})|_{x_D=0}. \tag{E3}$$

The dimensionless stream mass-balance condition is transformed as

$$p\tilde{\tilde{s}}_{D,r} = \beta_D^*(\tilde{\tilde{s}}_D|_{x_D=0} - \tilde{\tilde{s}}_{D,r}). \tag{E4}$$

Solving equation (E4), one can obtain

$$\tilde{\tilde{s}}_{D,r} = \frac{\beta_D^*}{p+\beta_D^*}\,\tilde{\tilde{s}}_D|_{x_D=0}\,. \tag{E5}$$

To deal with the Dirac Delta function in equation (E1), the jump conditions in $x_D = 1$ are imposed, that is,

$$\tilde{\tilde{s}}_D|_{x_D=1^+} = \tilde{\tilde{s}}_D|_{x_D=1^-}\,, \tag{E6}$$

$$\left.\frac{\mathrm{d}\tilde{\tilde{s}}_D}{\mathrm{d}x_D}\right|_{x_D=1^+} = \left.\frac{\mathrm{d}\tilde{\tilde{s}}_D}{\mathrm{d}x_D}\right|_{x_D=1^-} - \frac{2}{p}, \tag{E7}$$

Therefore, The general solutions for $\tilde{\tilde{s}}_{D,L}$ and $\tilde{\tilde{s}}_{D,R}$ are

$$\tilde{\tilde{s}}_D = \begin{cases} C_1 e^{\eta x_D} + C_2 e^{-\eta x_D} & x_D > 1, \text{ and} \\ C_3 e^{\eta x_D} + C_4 e^{-\eta x_D} & x_D \in [0,1), \end{cases} \tag{E8}$$

where $C_1 - C_4$ are undetermined coefficients. From the farfield boundary condition, it follows that $C_1 \equiv 0$. Imposing equations (E3) and (E4) on equation (E8), it can be shown that

$$C_2 = \frac{2}{p\eta\Delta_3}[(p+\beta_D^*)\eta\cosh(\eta) + p\beta_D\sinh(\eta)], \tag{E9}$$

$$C_3 = \frac{2e^{-\eta}(p+\beta_D^*)}{p\Delta_3}, \tag{E10}$$

$$C_4 = \frac{2\beta e^{-\eta}}{\eta\Delta_3}, \tag{E11}$$

where $\Delta_3 = \eta(p+\beta_D^*) + p\beta_D$. From the coefficients obtained above, the dimensionless aquifer and stream drawdown solutions for FPS are given in equations (27) and (28), respectively.

Appendix F: Model Verification

To check the correctness of the analytical solutions developed above, a verification exercise was undertaken by comparing these solutions with a numerical solution based on the FEM. A 3D FEM model was built for comparison with the NPS case and to

evaluate the significance of vertical flow. The stream overlying the aquifer was allowed to drain through the streambed and generate vertical flow. The domain is set as above with $z_D \in [0, 1.5]$. As mentioned above, the conceptual model comprises three isotropic layers, namely the aquifer layer with $z_D \in [0, 1]$, the streambed layer with $z_D \in (1, 1 + b'_D]$ with $x_D \in [-W_D, 0]$ and $y_D \in [0, 10^5]$, and the stream layer with $z_D \in (1 + b'_D, 1.5]$ with $x_D \in [-W_D, 0]$ and $y_D \in [0, 10^5]$. The drawdown computed with the 3D FEM model is vertically averaged. Finer meshes were assigned near the stream and pumping well, while a coarser mesh was used elsewhere. The hydraulic parameter values used for the comparison were set to $C_{D,r} = 25$, $\beta_D = 10$, $b'_D = 0.01$, and $W_D = 0.5$. The streambed storage was set the same as the aquifer and $K' = 0.1K_x$.

In the case of the FPS with a fully penetrating pumping well, the vertical flow is negligible and a 2D model in the (x_D, y_D) plane is sufficient to describe the flow behavior. The numerical solution was developed in a domain with $x_D \in [-10^5, 10^5]$ and $y_D \in [0, 10^5]$. The flow domain was divided into multiple zones: the pumped aquifer zone: $x_D \in [0, 10^5]$, aquifer zone on the far side: $x_D \in [-2b'_D, -10^5]$, the stream zone: $x_D \in [-b'_D, -b'_D - W_D)$, and streambed zones: $x_D \in [0, -b'_D)$ and $[-b'_D - W_D, -2b'_D - W_D)$, where b'_D is the dimensionless streambed thickness defined as b'/R. Figure F1 shows the aquifer drawdown curves predicted by the (a) NPS and (b) FPS solutions versus the FEM solution. The observation points were established at $(x_D, y_D) = (0.1, 0), (0.25, 0), (0.5, 0)$. The results show that the semi-analytical and FEM solutions agree well with negligible residuals. Additionally, Butler Jr et al. (2001) tested the assumptions of the NPS model by comparing it with the seven-layer MODFLOW model. They found that the NPS assumptions are valid when the relative penetration (ratio of stream penetration to aquifer thickness) is less than 85%. For the Cal Poly stream-aquifer system that motivated this study, the relative penetration is 50%.

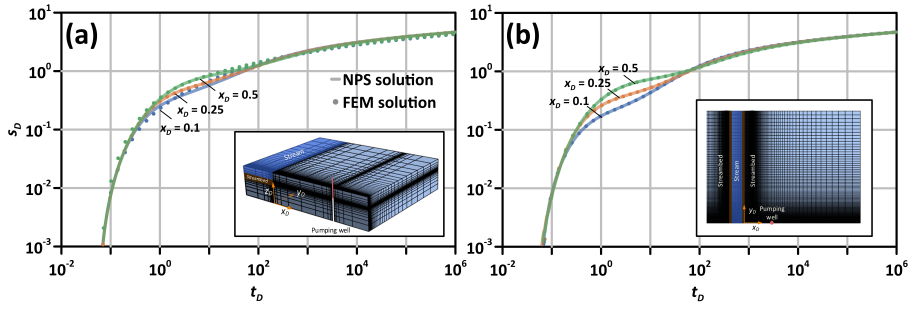

Figure F1. Comparison of the aquifer drawdown curves predicted by the (a) NPS and (b) FPS solutions and FEM solutions based on 3D and 2D model. The visual representations of the meshes near the well used in the 3D and 2D FEM models are included in the bottom right corner of the figure.

Appendix G: Evaluation of the Depletion Integral

In Figure G1 we compare the $Q_{D,r}$ curves with $L_D = R_{D,\infty}$ given above versus the arbitrary upper bound of $L_D = 10^5$. The two curves are nearly identical with a maximum relative error (RE) of less than 10% at the early time. For $t_D > 1$, the RE is less than 2%. The CPU time shows that the setting $L_D = R_{D,\infty}$ computes faster than the use of $L_D = 10^5$.

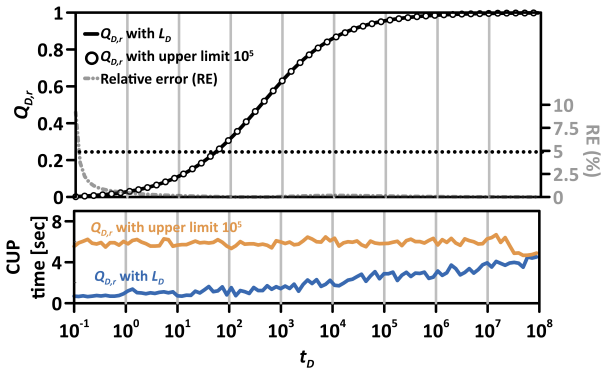

Figure G1. The $Q_{D,r}$ curves showing evaluated depletion integral using upper limit of L_D (solid line) and 10^5 (circle symbol), as well as the relative error (RE) curve with a horizontal line standing for 5% RE. The curves of used CPU time for these two cases are also included below.

Author contributions. BM wrote, reviewed, and edited the manuscript, planned the methodology and the formal analysis; YFL assisted to edit the manuscript, analyze the data, and perform the data virtualization; HLY and HTT analyzed the data; SG collected the data.

Competing interests. The authors declare that they have no conflict of interest.

Acknowledgements. Funded in part by a California State University's Agricultural Research Initiative (ARI) grant.

References

Asadi-Aghbolaghi, M. and Seyyedian, H.: An analytical solution for groundwater flow to a vertical well in a triangle-shaped aquifer, Journal of Hydrology, 393, 341–348, https://doi.org/https://doi.org/10.1016/j.jhydrol.2010.08.034, 2010.

Bochever, F.: Evaluation of well-field yield in alluvial aquifers: The impact of a partially penetrating stream, Proceedings of VODGEO (Hydrogeology), 13, 84–115, 1966.

Bourdet, D., Whittle, T., Douglas, A., and Pirard, Y.: A new set of type curves simplifies well test analysis, World oil, 196, 95–106, 1983.

Bowen, J., Kroeger, K., Tomasky, G., Pabich, W., Cole, M., Carmichael, R., and Valiela, I.: A review of land–sea coupling by groundwater discharge of nitrogen to New England estuaries: Mechanisms and effects, Applied geochemistry, 22, 175–191, https://doi.org/https://doi.org/10.1016/j.apgeochem.2006.09.002, 2007.

Butler Jr, J. J., Zlotnik, V. A., and Tsou, M.-S.: Drawdown and stream depletion produced by pumping in the vicinity of a partially penetrating stream, Groundwater, 39, 651–659, https://doi.org/https://doi.org/10.1111/j.1745-6584.2001.tb02354.x, 2001.

Butler Jr, J. J., Zhan, X., and Zlotnik, V. A.: Pumping-induced drawdown and stream depletion in a leaky aquifer system, Groundwater, 45, 178–186, https://doi.org/https://doi.org/10.1111/j.1745-6584.2006.00272.x, 2007.

Chan, Y.: Improved image-well technique for aquifer analysis, Journal of Hydrology, 29, 149–164, https://doi.org/https://doi.org/10.1016/0022-1694(76)90011-1, 1976.

Chow, V. T.: On the determination of transmissibility and storage coefficients from pumping test data, Eos, Transactions American Geophysical Union, 33, 397–404, https://doi.org/https://doi.org/10.1029/TR033i003p00397, 1952.

Cooper Jr, H. and Jacob, C. E.: A generalized graphical method for evaluating formation constants and summarizing well-field history, Eos, Transactions American Geophysical Union, 27, 526–534, https://doi.org/https://doi.org/10.1029/TR027i004p00526, 1946.

De Smedt, F.: Analytical solution for constant-rate pumping test in fissured porous media with double-porosity behaviour, Transport in Porous Media, 88, 479–489, https://doi.org/https://doi.org/10.1007/s11242-011-9750-9, 2011.

Ferris, J. G., Knowles, D. B., Brown, R., and Stallman, R. W.: Theory of aquifer tests, US Government Printing Office Denver, CO, USA, 1962.

Ferroud, A., Chesnaux, R., and Rafini, S.: Insights on pumping well interpretation from flow dimension analysis: The learnings of a multi-context field database, Journal of hydrology, 556, 449–474, https://doi.org/https://doi.org/10.1016/j.jhydrol.2017.10.008, 2018.

Ferroud, A., Rafini, S., and Chesnaux, R.: Using flow dimension sequences to interpret non-uniform aquifers with constant-rate pumping-tests: A review, Journal of Hydrology X, 2, 100 003, https://doi.org/https://doi.org/10.1016/j.hydroa.2018.100003, 2019.

Foglia, L., McNally, A., and Harter, T.: Coupling a spatiotemporally distributed soil water budget with stream-depletion functions to inform stakeholder-driven management of groundwater-dependent ecosystems, Water Resources Research, 49, 7292–7310, https://doi.org/https://doi.org/10.1002/wrcr.20555, 2013.

Fox, G. A., DuChateau, P., and Dumford, D. S.: Analytical model for aquifer response incorporating distributed stream leakage, Groundwater, 40, 378–384, https://doi.org/https://doi.org/10.1111/j.1745-6584.2002.tb02516.x, 2002.

Glover, R. E. and Balmer, G. G.: River depletion resulting from pumping a well near a river, Eos, Transactions American Geophysical Union, 35, 468–470, https://doi.org/https://doi.org/10.1029/TR035i003p00468, 1954.

Grigoryev, V.: The effect of streambed siltation on well-field yield in alluvial aquifers, Water Supply and Sanitation, 6, 10–l, 1957.

Haberman, R.: Applied partial differential equations with Fourier series and boundary value problems, Pearson Higher Ed, 2012.

Hantush, M. S.: Wells near streams with semipervious beds, Journal of Geophysical Research, 70, 2829–2838, https://doi.org/https://doi.org/10.1029/JZ070i012p02829, 1965.

Hantush, M. S. and Jacob, C. E.: Non-steady radial flow in an infinite leaky aquifer, Eos, Transactions American Geophysical Union, 36, 95–100, https://doi.org/https://doi.org/10.1029/TR036i001p00095, 1955.

Harbaugh, A. W.: MODFLOW-2005, the US Geological Survey modular ground-water model: the ground-water flow process, US Department of the Interior, US Geological Survey Reston, VA, 2005.

Huang, C.-S., Yang, T., and Yeh, H.-D.: Review of analytical models to stream depletion induced by pumping: Guide to model selection, Journal of Hydrology, 561, 277–285, https://doi.org/https://doi.org/10.1016/j.jhydrol.2018.04.015, 2018.

Hunt, B.: Unsteady stream depletion from ground water pumping, Groundwater, 37, 98–102, https://doi.org/https://doi.org/10.1111/j.1745-6584.1999.tb00962.x, 1999.

Hunt, B.: Field-data analysis for stream depletion, Journal of Hydrologic Engineering, 8, 222–225, https://doi.org/https://doi.org/10.1061/(ASCE)1084-0699(2003)8:4(222), 2003.

Hunt, B.: Stream depletion in a two-layer leaky aquifer system, Journal of Hydrologic Engineering, 14, 895–903, https://doi.org/https://doi.org/10.1061/(ASCE)HE.1943-5584.0000063, 2009.

Intaraprasong, T. and Zhan, H.: A general framework of stream–aquifer interaction caused by variable stream stages, Journal of Hydrology, 373, 112–121, https://doi.org/https://doi.org/10.1016/j.jhydrol.2009.04.016, 2009.

Jenkins, C. T.: Techniques for Computing Rate and Volume of Stream Depletion by Wells, Groundwater, 6, 37–46, https://doi.org/https://doi.org/10.1111/j.1745-6584.1968.tb01641.x, 1968.

Johann, F.: pyts.decomposition documentation, 2021.

Kollet, S. J. and Zlotnik, V. A.: Stream depletion predictions using pumping test data from a heterogeneous stream–aquifer system (a case study from the Great Plains, USA), Journal of Hydrology, 281, 96–114, 2003.

Kwon, H.-I., Koh, D.-C., Jung, Y.-Y., Kim, D.-H., and Ha, K.: Evaluating the impacts of intense seasonal groundwater pumping on stream–aquifer interactions in agricultural riparian zones using a multi-parameter approach, Journal of Hydrology, 584, 124 683, https://doi.org/https://doi.org/10.1016/j.jhydrol.2020.124683, 2020.

Laszuk, D.: PyEMD documentation, 2020.

Lin, Y.-C. and Yeh, H.-D.: An Analytical Model With a Generalized Nonlinear Water Transfer Term for the Flow in Dual-Porosity Media Induced by Constant-Rate Pumping in a Leaky Fractured Aquifer, Water Resources Research, 57, e2020WR029 186, https://doi.org/https://doi.org/10.1029/2020WR029186, 2021.

Lin, Y.-C., Huang, C.-S., and Yeh, H.-D.: Analysis of unconfined flow induced by constant rate pumping based on the lagging theory, Water Resources Research, 55, 3925–3940, https://doi.org/https://doi.org/10.1029/2018WR023893, 2019.

Malama, B.: Alternative linearization of water table kinematic condition for unconfined aquifer pumping test modeling and its implications for specific yield estimates, Journal of Hydrology, 399, 141–147, https://doi.org/https://doi.org/10.1016/j.jhydrol.2010.11.007, 2011.

Mishra, P. K. and Neuman, S. P.: Improved forward and inverse analyses of saturated-unsaturated flow toward a well in a compressible unconfined aquifer, Water Resources Research, 46, https://doi.org/https://doi.org/10.1029/2009WR008899, 2010.

Neuman, S. P.: Effect of partial penetration on flow in unconfined aquifers considering delayed gravity response, Water Resources Research, 10, 303–312, https://doi.org/https://doi.org/10.1029/WR010i002p00303, 1974.

Povstenko, Y.: Linear fractional diffusion-wave equation for scientists and engineers, Springer, 2015.

Prudic, D. E., Konikow, L. F., and Banta, E. R.: A new streamflow-routing (SFR1) package to simulate stream-aquifer interaction with MODFLOW-2000, 2004.

Refsgaard, J. C., Storm, B., and Clausen, T.: Système Hydrologique Europeén (SHE): review and perspectives after 30 years development in distributed physically-based hydrological modelling, Hydrology Research, 41, 355, https://doi.org/https://doi.org/10.2166/nh.2010.009, 2010.

Stehfest, H.: Algorithm 368: Numerical inversion of Laplace transforms [D5], Communications of the ACM, 13, 47–49, https://doi.org/https://doi.org/10.1145/361953.361969, 1970.

Streltsova, T. D.: Well pressure behavior of a naturally fractured reservoir, Society of Petroleum Engineers Journal, 23, 769–780, https://doi.org/https://doi.org/10.2118/10782-PA, 1983.

Theis, C. V.: The relation between the lowering of the piezometric surface and the rate and duration of discharge of a well using ground-water storage, Eos, Transactions American Geophysical Union, 16, 519–524, https://doi.org/https://doi.org/10.1029/TR016i002p00519, 1935.

Theis, C. V.: The effect of a well on the flow of a nearby stream, Eos, Transactions American Geophysical Union, 22, 734–738, https://doi.org/https://doi.org/10.1029/TR022i003p00734, 1941.

Tolley, D., Foglia, L., and Harter, T.: Sensitivity Analysis and Calibration of an Integrated Hydrologic Model in an Irrigated Agricultural Basin With a Groundwater-Dependent Ecosystem, Water Resources Research, 55, 7876–7901, https://doi.org/https://doi.org/10.1029/2018WR024209, 2019.

Warren, J. and Root, P. J.: The behavior of naturally fractured reservoirs, Society of Petroleum Engineers Journal, 3, 245–255, https://doi.org/https://doi.org/10.2118/426-PA, 1963.

Winter, T. C., Harvey, J. W., Franke, O. L., and Alley, W. M.: Ground water and surface water: a single resource, vol. 1139, US Geological Survey, 1998.

Yu, H.-L. and Chu, H.-J.: Understanding space–time patterns of groundwater system by empirical orthogonal functions: a case study in the Choshui River alluvial fan, Taiwan, Journal of Hydrology, 381, 239–247, https://doi.org/https://doi.org/10.1016/j.jhydrol.2009.11.046, 2010.

Zipper, S. C., Dallemagne, T., Gleeson, T., Boerman, T. C., and Hartmann, A.: Groundwater pumping impacts on real stream networks: Testing the performance of simple management tools, Water Resources Research, 54, 5471–5486, https://doi.org/https://doi.org/10.1029/2018WR022707, 2018.

Zlotnik, V. A.: A concept of maximum stream depletion rate for leaky aquifers in alluvial valleys, Water Resources Research, 40, https://doi.org/https://doi.org/10.1029/2003WR002932, 2004.

Zlotnik, V. A. and Tartakovsky, D. M.: Stream depletion by groundwater pumping in leaky aquifers, Journal of Hydrologic Engineering, 13, 43–50, https://doi.org/https://doi.org/10.1061/(ASCE)1084-0699(2008)13:2(43), 2008.

Zlotnik, V. A., Huang, H., and Butler Jr, J. J.: Evaluation of stream depletion considering finite stream width, shallow penetration, and properties of streambed sediments, 2nd International Conference on Water Resources & Environment Research, 1999.